J. Fluid Mech. (2001), *vol.* 427, *pp.* 131–165. Printed in the United Kingdom

On the structure of a Taylor column driven by a buoyant parcel in an unbounded rotating fluid

By DAVID E. LOPER

Geophysical Fluid Dynamics Institute, Florida State University, Tallahassee, FL 32306, USA

(Received 21 October 1999 and in revised form 2 August 2000)

The velocity and pressure fields produced in a homogeneous rapidly rotating fluid driven by an isolated buoyant parcel are investigated. Gravity and rotation are allowed to have arbitrary orientations and the parcel shape is assumed Gaussian. Inertial forces and time-dependent effects are ignored. The linear problem is easily solved by three-dimensional Fourier transform, and the inversion is facilitated by assuming the Ekman number, E, to be very small. In this limit the fields form a Taylor column extended in the direction of the rotation axis. In the absence of rigid boundaries no boundary layers occur. The velocity and pressure in the vicinity of the parcel are found in closed form while elsewhere (within the Taylor column) they are expressed in terms of relatively simple scalar integrals which are easily evaluated.

Within the buoyant parcel, the momentum balance is baroclinic, involving Coriolis, pressure and buoyancy forces. Outside the parcel, the balance is geostrophic at unit order. The viscous force is important at order E and determines the axial structure of the Taylor column. In contrast to the case of flow driven by a rigid body, no 'Taylor slug' of recirculating flow occurs. The velocity and pressure decay algebraically with distance from the parcel, with the scale of variation being a/E in the axial direction and a in the radial direction, where a is the parcel radius. In the vicinity of the parcel, the return flow occurs in a broad region surrounding the parcel. The structure of flow in the vicinity of the parcel is independent of the Ekman number. This return flow sweeps the fringes of the parcel backward, making the net rise speed significantly slower than that of a rigid sphere of identical buoyancy. The return flow also acts to deform the parcel; this deformation is quantified.

1. Introduction

The behaviour of flows in homogeneous, rapidly rotating fluids has fascinated fluid dynamicists since the prediction and verification of Taylor columns (Proudman 1916; Taylor 1922, 1923). In such systems the dominant momentum balance is geostrophic and the Taylor–Proudman theorem states that the velocity is invariant in the direction of the rotation vector. There are several reasons for the continuing interest in these flows. One is a desire to better understand the 'action at a distance' manifested by the Taylor–Proudman theorem and how this constraint is mediated by other, weaker forces. Mediation by the viscous force produces variation of the Taylor column in the direction of the rotation axis, i.e. the *axial* direction, on the scale $\Omega a^3/\nu$ where Ω is the rotation rate, ν is the kinematic viscosity and a is the spatial scale of the localized disturbance in the plane normal to the rotation axis. This axial variation is

referred to as *structure* of the Taylor column in what follows. A second motive is the desire to understand and quantify the flow field in the vicinity of that body and to determine what controls that flow. A third is the desire to understand and quantify the relation between the force on a body (either rigid or fluid) and its velocity. Each of these issues is addressed in what follows.

If the motions are sufficiently slow and steady that inertial forces are negligible, the geostrophic balance and axial invariance of a Taylor column is modified by the action of the viscous force. This modification takes two distinct forms depending on the axial extent of the fluid, measured from a localized source of motion such as an isolated rigid body or buoyant parcel. If the axial extent is much less than $2\Omega a^3/\nu$, then viscosity acts to create and maintain thin boundary layers: Ekman layers adjacent to impenetrable boundaries not parallel to the rotation axis and Stewartson $E^{1/3}$ and $E^{1/4}$ layers parallel to the rotation axis, where E is defined by (1.1) below. In this case the fluid is said to be contained and the associated columns and layers are well studied and understood (e.g. see Greenspan 1968; Hide, Ibbetson & Lighthill 1968; Moore & Saffman 1968, 1969; Bush, Stone & Bloxham 1995).

On the other hand, if the axial extent is much larger than $2\Omega a^3/\nu$, then viscosity causes a slow variation in the structure of the Taylor column with axial distance. This large-scale structure of a Taylor column is rather poorly understood, in large part because the mathematical problem posed by an axially unconfined fluid appears more difficult than that posed by a confined fluid. In what follows attention is focused on rapidly rotating flows in unconfined fluids.

Such flows can occur in a variety of natural and engineering settings, including the atmosphere, oceans, Earth's core and centrifuges. In these settings motions are typically driven by a parcel of fluid with an excess or deficit of buoyancy. In spite of this, nearly all previous studies (with the exception of Bush, Stone & Bloxham 1992, 1995) of Taylor-column structure in axially unbounded fluids have concentrated on effects produced by rigid particles or bodies having a prescribed motion relative to the rotating fluid, principally motion parallel to the axis of rotation. Unfortunately rapidly rotating flows driven by rigid bodies are described by dual-integral equations which are difficult to solve if the Taylor number is very large and this has limited progress toward understanding the Taylor-column structure. We shall see in the following sections that flow driven by an isolated buoyant parcel is relatively simpler to solve.

The characterization of a rotating fluid as axially confined or unconfined depends on the size of the disturbance; any disturbance having a horizontal scale smaller than $(l\nu/2\Omega)^{1/3}$, where l is the axial extent of the fluid, is axially unconfined. For example, the typical depth of the ocean is 5×10^3 m and the kinematic viscosity of water is roughly $10^{-6}\,\mathrm{m^2\,s^{-1}}$. With $\Omega = 7 \times 10^{-5}\,\mathrm{s^{-1}}$, a disturbance smaller than 3 m in horizontal scale is essentially unconfined at mid-depth in the ocean. A similar result obtains for the atmosphere with a depth again of several kilometres and a kinematic viscosity of $1.3 \times 10^{-5}\,\mathrm{m^2\,s^{-1}}$. In Earth's outer core, with a depth of 2×10^6 m and a kinematic viscosity of $5 \times 10^{-7}\,\mathrm{m^2\,s^{-1}}$, say, this calculation yields a maximum size of 20 m for an unconfined disturbance.†

The extreme length of the Taylor column is responsible for the rather limited applicability of those parts of the analysis presented below which deal with the structure of the Taylor column. However, solutions for flow and pressure in the vicinity of the parcel, presented in § 7, are believed to have a significantly wider range

† The fluid of the outer core is also subject to the Lorentz force; this quantification is for illustration only.

of validity. Preliminary investigations have shown that those solutions are, remarkably, independent of the nature of the secondary force (e.g. viscous, inertial, stratification or Lorentz) which balances the Coriolis force, provided only that the Coriolis force remains dominant. The length of the Taylor column is due to the weakness of the viscous force relative to the Coriolis force (see § 2.1). The flow adopts a configuration such that a small departure from precise geostrophy may be balanced by the weak viscous force. This departure is locally small, requiring cumulative action over a long axial distance to modify the form of the Taylor column. The severe conditions on the applicability of the analysis of Taylor-column structure, documented in the previous paragraph, will be relaxed as additional, stronger forces (e.g. inertial, Lorentz or stratification) are taken into account and the axial extent of the Taylor column correspondingly decreases. These forces will be investigated in subsequent studies.

1.1. *Scope of the present study*

This paper considers the velocity field and pressure generated in a rapidly rotating, unbounded fluid driven by an isolated buoyant parcel. As will be seen, the associated mathematical problem is somewhat simpler to analyse and solve than that posed by either a rigid body in an unconfined fluid or a fluid parcel within a confined fluid. This simplicity allows consideration of configurations in which gravity and rotation have arbitrary orientations.

In what follows the fluid is assumed to be rotating sufficiently rapidly that the Ekman number is much smaller than unity:

$$E = \frac{\nu}{2\Omega a^2} \ll 1. \tag{1.1}$$

This provides a small parameter which will be used to advantage. The Rossby number,

$$R_o = \frac{U}{2\Omega a}, \tag{1.2}$$

where U is the characteristic convective speed, is assumed to be sufficiently small that the inertial force is smaller than the viscous force. This condition is sensitive to the relative orientation of rotation and gravity. When the two vectors are aligned, it is sufficient to specify that $R_o \ll 1$. However, when they are not aligned, it is shown in Appendix A that a more restrictive condition is necessary: $R_o \sin\theta \ll E$.
Altogether,

$$R_o \ll \{E/\sin\theta, 1\}, \tag{1.3}$$

where θ is the acute angle between the rotation axis and the gravity vector: $\cos\theta = |\hat{\boldsymbol{g}}\cdot\hat{\boldsymbol{\Omega}}|$. Here $\hat{\boldsymbol{\Omega}}$ and $\hat{\boldsymbol{g}}$ are unit vectors pointing in the directions of the rotation axis and gravity vector, respectively. If rotation and gravity are aligned, $\theta = 0$ and the constraint in (1.3) involving θ is automatically satisfied. Invariably these vectors are aligned in laboratory experiments so that constraint is moot. However, in natural settings θ represents the co-latitude and the constraint involving θ in (1.3) is strong, except near the North and South Poles. In rapidly rotating, buoyancy-driven flows the characteristic speed, U, results from the balance between Coriolis and buoyancy forces:

$$U = \frac{(\Delta\rho)g}{\rho 2\Omega}, \tag{1.4}$$

where g is the magnitude of the local acceleration due to gravity, ρ is the density of the ambient fluid and $\Delta\rho$ is a measure of the density deficit (or excess) of the parcel. ($\Delta\rho$ is positive for a density deficit.) Using (1.5) the portion of constraint (1.3)

involving θ may be expressed as

$$\sin\theta \ll \frac{2\Omega v\rho}{ga\Delta\rho}. \tag{1.5}$$

This is in fact a severe constraint, as the right-hand side of (1.6) is typically very small.

Often the Taylor number, $\mathscr{T}$, and Reynolds number, R_e, are used in place of the Ekman and Rossby numbers. These two sets are related by $\mathscr{T} = 1/E$ and $R_e = R_o/E$, and the conditions on the validity of the following analysis are $\mathscr{T} \gg 1$ and $R_e \ll \{1/\sin\theta, \mathscr{T}\}$. The set E, R_o is used in the following analysis.

1.2. *Organization of the paper*

The goals of the analysis and the relation to previous work are discussed in § 2. The mathematical problem is formulated in § 3 and is non-dimensionalized and linearized on the basis of condition (1.3). With the flow driven by a fluid parcel in an unbounded domain, there are no rigid boundaries and the (linearized) governing equations are valid everywhere. This problem is amenable to solution by a three-dimensional Fourier transform. An important contribution of this paper is the description of a procedure for inverting the Fourier solution; the details of this are presented in Appendix B. Two of the inversion integrals can be performed for all values of spatial position, $\boldsymbol{x}$. The result is an expression for the velocity vector in terms of a relatively simple set of single integrals, given in § 4.1. The associated pressure field is found in § 4.2. Simplified forms of the solutions are described in § 4.3; these are presented in equations (4.20) and (4.21).

The solutions described in § 4.3 involve single integrals having the meridional-plane coordinates of physical space as parameters. The number of parameters is reduced to one, making the intergrals amenable to graphical representation, on the modal axis (see § 5) and far from the parcel (see § 6). Moreover, the integrals may be evaluated exactly in the vicinity of the parcel; these solutions are presented in § 7. The rise velocity of the parcel is evaluated in § 8, and is compared to the velocity of a buoyant rigid parcel.

The problem considered in this paper is kinematic, in that the buoyancy distribution is prescribed. In reality such a distribution will be deformed by the velocity field. This deformation is investigated in § 9, and it is found in § 9.1 that the solution obtained in § 4 is insensitive to this deformation if rotation and gravity are aligned. The solution is more sensitive to deformation in the case that rotation and gravity are not aligned; in § 9.2 a generalized form of the buoyancy distribution is suggested which may yield a more robust solution. The analysis is summarized and its implications are discussed in § 10.

2. Goals of the analysis and relation to previous work

In the following sections, attention is focused on the three issues mentioned in the introductory paragraph: structure of the Taylor column, flow and pressure near the body and force–velocity relation. These issues and the attention they have received in the past are discussed in the following subsections.

2.1. *Taylor-column structure* (*at axial distance* a/E)

The Taylor–Proudman theorem derives from the curl of the momentum equation. In the case that the momentum balance involves only Coriolis, pressure and viscous forces, this states that

$$2(\boldsymbol{\Omega}\cdot\nabla)\boldsymbol{u} = \nu\nabla^2\nabla\times\boldsymbol{u}. \tag{2.1}$$

We infer from this that $\partial/\partial x_\Omega = O(\nu/2\Omega a^3) = O(E/a)$ where $x_\Omega = \hat{\boldsymbol{\Omega}}\cdot\boldsymbol{x}$, and a caret denotes a unit vector, e.g. $\boldsymbol{\Omega} = \Omega\hat{\boldsymbol{\Omega}}$. To dominant order in powers of E the right-hand side of (2.1) is negligibly small, so that variations in the direction of rotation are weak. This conclusion holds provided that the scale of variation normal to rotation is characterized by the lateral scale of the body or parcel, i.e. $x_\perp = O(a)$. This is certainly the case close to the body or parcel. However, if the axial and normal variations are such that

$$\nu(\Delta x_\Omega) = O[2\Omega(\Delta x_\perp)^3], \tag{2.2}$$

then viscous and Coriolis forces are in balance. This balance will yield the Stewartson $E^{1/3}$ layer of confined flows provided the axial extent of the fluid, Δx_Ω, is limited and prescribed; in this case $\Delta x_\perp$ is a small normal (i.e. radial) distance. Alternatively, if $\Delta x_\perp \approx a$, the usual scaling of the Taylor column is obtained: $\Delta x_\Omega \approx 2\Omega a^3/\nu = a/E$.

The asymptotic Taylor-column structure (on an axial scale $> a/E$) is sensitive only to the total buoyancy force exerted by a fluid parcel or to the total drag force exerted by a rigid parcel and is insensitive to the detailed distribution of these forces on the scale of the parcel or body. Relation (2.2) provides a similarity variable for analysing this asymptotic structure. It also is of use in analysing the full behaviour of rapidly rotating flow driven by a point force (e.g. see § 4 of Herron, Davis & Bretherton 1975, and § 3.4 of Tanzosh & Stone 1994).

2.2. *Flow near the parcel*

A characteristic feature of Taylor columns driven by rigid bodies moving parallel to the rotation axis at low Rossby numbers is the occurrence of a column of trapped fluid moving with the body (Taylor 1922; Stewartson 1952; Long 1953; Pritchard 1969; Maxworthy 1970; Tanzosh & Stone 1994; Vedensky & Ungarish 1994; Ungarish & Vedensky 1995). The axial extent of this trapped fluid, referred to as the Taylor slug, is often used as a measure of the length of the Taylor column. It is seen in § 5 that the situation is quite different for a Taylor column created by a fluid parcel; no Taylor slug occurs. A possible reason for this difference in flow structure is presented in that section.

There are additional differences in flow structures driven by a rigid body or a fluid parcel. Flow driven by a rigid body is characterized by Ekman boundary layers on the body and Stewartson $E^{1/3}$ and $E^{1/4}$ layers on the tangent cylinder. Also, the swirl flow on that cylinder becomes unbounded as the inviscid limit is approached (Stewartson 1952). It turns out that the flow created by a buoyant parcel in an unbounded fluid lacks viscous boundary layers of any kind; Ekman and Stewartson layers owe their existence to the presence of rigid boundaries. The flow driven by a buoyant parcel is 'softer' than that driven by a rigid body in that there is no singular behaviour on the tangent cylinder. In fact, parcel-driven flow has no clearly defined tangent cylinder.

Some form of dual integral problem is inevitably encountered in the analysis of flow driven by a finite rigid body (e.g. Vedensky & Ungarish 1994; Tanzosh & Stone 1995; Vedensky & Ungarish 1995). The best solution method for such problems, Tranter's method (Tranter 1966), although valid for all Taylor numbers, is poorly convergent at high Taylor number. The method presented below is asymptotically valid for large Taylor number (small Ekman number) and is in effect complementary to Tranter's method. The flow driven by a buoyant parcel is somewhat easier to solve than the corresponding flow driven by a rigid body; a complete analytic solution for the flow in the vicinity of a buoyant parcel is presented in § 7.

Equation (2.1) is the simplest form of the Taylor–Proudman theorem, in that all small forces, other than viscosity, have been ignored. Additional forces which might enter this balance include inertial, buoyancy (due to ambient stratification) and

Lorentz. A remarkable and surprising feature of this problem is that the flow and pressure near the buoyant parcel (presented in § 7) are independent of the Ekman number. This implies that these near-parcel solutions will remain valid if forces other than viscous balance the Coriolis force. Since the length of the Taylor column is proportional to the ratio of the Coriolis to the secondary force, it is possible that the Taylor column will be significantly shorter when forces other than viscous are important. This implies that the solution presented in § 7 may have a larger range of validity than implied by constraint (1.3). This conjecture is beyond the scope of the present paper, and will be investigated subsequently.

2.3. *Force–drag relation*

In flows driven by rigid bodies, typically the velocity of the body is specified and the force is calculated as part of the solution. In the present case of flow driven by a buoyant parcel, the situation is reversed: the force on the parcel is specified and the velocity of the parcel is calculated. Stewartson (1952) first obtained a relation between the drag, D_p, and rise speed, U, of an axisymmetric rigid body moving parallel to the rotation axis:

$$D_p = \tfrac{16}{3}\rho\Omega U a^3, \tag{2.3}$$

where a is the radius of the circular 'foot-print' of the body in the plane normal to the rotation axis. Maxworthy (1970) determined experimentally that the drag on a sphere is 1.52 times this theoretical value. The reason for this discrepancy is unknown. If the body were a sphere having a density deficit or excess of $\Delta\rho$ with gravity and rotation parallel, then it would rise or sink due to its buoyancy force with speed

$$U_p = \frac{\pi}{2}\left(\frac{\Delta\rho}{\rho}\right)\frac{g}{2\Omega}. \tag{2.4}$$

Stewartson (1953; see also Tanzosh & Stone 1995) determined that a sphere moving normal to rotation experiences a drag force

$$D_\perp = \frac{32\pi^2}{3(16+\pi^2)}\rho\Omega U a^3, \tag{2.5}$$

and a lateral force (lift)

$$D_L = \frac{8\pi^3}{3(16+\pi^2)}\rho\Omega U a^3. \tag{2.6}$$

(In comparing (2.5) and (2.6) with (6.26) and (6.27) of Stewartson (1953), recall that $\Omega = \frac{1}{2}$ in his formulation.) If the body were a sphere having a density deficit or excess of $\Delta\rho$ and gravity and rotation were perpendicular, then it would rise or sink due to its buoyancy force with speed

$$U_\perp = \frac{16\pi}{16+\pi^2}\left(\frac{\Delta\rho}{\rho}\right)\frac{g}{2\Omega}, \tag{2.7}$$

and presumably move laterally at $\pi/4$ this speed.

The rise of a buoyant parcel in an unbounded fluid has been investigated by Moffatt & Loper (1994) in the case that the fluid is electrically conducting and in the presence of an external magnetic field. The parcel was assumed to be spherical and to have a Gaussian density distribution. In the limit that magnetic effects are negligible,

the velocity field at the centre of the parcel was found to be

$$\boldsymbol{u}(0) = \left(\frac{\Delta\rho}{\rho}\right)\frac{g}{2\Omega}\left\{-\frac{\pi}{4}[\hat{\boldsymbol{g}} + (\hat{\boldsymbol{g}}\cdot\hat{\boldsymbol{\Omega}})\hat{\boldsymbol{\Omega}}] + \hat{\boldsymbol{\Omega}}\times\hat{\boldsymbol{g}}\right\}. \tag{2.8}$$

This velocity consists of an in-plane motion, represented by the term on the right-hand side involving the square bracket and a motion out of the plane defined by $\hat{\boldsymbol{\Omega}}$ and $\hat{\boldsymbol{g}}$, represented by the last term on the right-hand side. The out-of-plane motion does not contribute to the rise speed of the parcel, but causes it to drift horizontally (specifically westward). When applied to geophysical problems, the rise speed predicted by (2.8) depends on the latitude, being twice as fast in polar regions as at the equator.

In the case that rotation and gravity are aligned, the velocity given by (2.8) is in agreement with (2.4), while if they are orthogonal, (2.8) yields

$$u_{\perp}(0) = \frac{\pi}{4}\left(\frac{\Delta\rho}{\rho}\right)\frac{g}{2\Omega}, \tag{2.9}$$

which is considerably slower than the orthogonal speed given by (2.7). The lift force acting on a fluid parcel also differs from that acting on a rigid body; see § 8.1.

The agreement between (2.8) and (2.4) in the aligned case appears at first glance to verify that Stewartson's drag formula (2.3) applies to fluid bodies as well as rigid. However, this conclusion rests on the assumption, made by Moffatt & Loper (1994), that the velocity of the fluid at the centre of the parcel is the same as that of the parcel as a whole. The validity of this assumption is questioned in § 8 and found wanting.

Bush *et al.* (1992) considered the motion of a deformable body, specifically an inviscid drop of liquid which is not miscible with the surrounding fluid, in a rapidly rotating fluid of limited axial extent. The associated surface tension gives the body a mechanism to balance the tendency of fluid motions to deform it, leading to an equilibrium, non-spherical shape of the drop. In a subsequent study (Bush *et al.* 1995), the problem was generalized to include the effect of non-zero viscosity in the drop and the effect of removing the axial boundaries to infinity. The behaviour of an axially unconfined drop was discussed qualitatively, but no mathematical analysis of the unbounded case was presented.

3. Formulation and transformed solution

The equations governing Taylor-column structure and flow are presented in dimensional form in § 3.1 and non-dimensionalized in § 3.2. The buoyancy function is specified in § 3.2. The problem is linearized and solved in Fourier-transform space in § 3.3.

3.1. *Conservation equations*

The flow associated with the rise of the parcel is assumed to be independent of time, when viewed in a frame of reference fixed to that parcel. The relative fluid velocity, $\boldsymbol{u}_r$, (i.e. the fluid velocity relative to the parcel), the laboratory-frame velocity, $\boldsymbol{u}_l$ (i.e. the fluid velocity relative to the quiescent ambient fluid) and the rise velocity, $\boldsymbol{U}_p$, of the parcel are related by

$$\boldsymbol{u}_r = \boldsymbol{u}_l - \boldsymbol{U}_p; \tag{3.1}$$

see figure 1. The rise velocity is to be determined as part of the solution; this is accomplished in § 8.

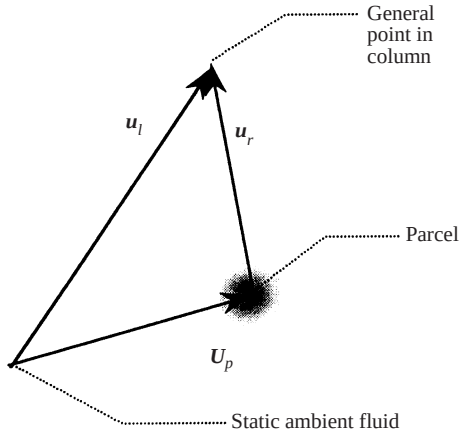

FIGURE 1. Illustration of the relation among the relative fluid velocity, $\boldsymbol{u}_r$, the laboratory-frame velocity, $\boldsymbol{u}_l$, and the rise velocity $\boldsymbol{U}_p$.

The Boussinesq equations governing the steady flow of an incompressible fluid of constant viscosity in a rotating environment, expressed in a rotating frame of reference fixed to the parcel, are

$$\rho_0[(\boldsymbol{U}_p - \boldsymbol{u}_l)\cdot\nabla]\boldsymbol{u}_l - 2\rho_0\boldsymbol{\Omega}\times\boldsymbol{u}_l + \rho_0\nu\nabla^2\boldsymbol{u}_l = \nabla p - (\rho-\rho_0)\boldsymbol{g}, \tag{3.2}$$

$$\nabla\cdot\boldsymbol{u}_l = 0. \tag{3.3}$$

Here p is the deviation from the hydrostactic pressure and the remaining notation is standard.

The factor $\rho - \rho_0$ is non-zero only within the buoyant parcel and is assumed to be prescribed and independent of time. In realilty the flow will deform the parcel, so that it will be of the prescribed shape only for some (small) interval of time. Deformation of the parcel by the flow is quantified in § 9.

The assumption of steady flow is valid provided that the Taylor column is established on a time short compared with the time of parcel motion and deformation. The Taylor column is established by the axial propagation and eventual viscous dissipation of inertial waves. Information regarding the position and shape of the fluid parcel is propagated with the group speed of internal waves, which is of order $a\Omega$. It takes a time of order $1/\Omega$ for information to propagate in the vicinity of the parcel and of order $a^2/\nu \approx 1/E\Omega$ on the scale of the Taylor column. The fluid parcel moves or deforms only slightly (compared with its radius) in time of order Ω^{-1} provided that $a/U \gg 1/\Omega$ or equivalently $R_o \ll 1$. But this is assured by condition (1.3). It follows that the flow in the vicinity of the parcel may be considered steady. A steady Taylor column is established in a time short compared with the parcel deformation time provided $R_o \ll E$, which is a more restrictive condition. However, it should be noted that the asymptotic structure of the Taylor column structure (on an axial scale larger than a/E) is sensitive only to the total applied force (e.g. see Herron *et al.* 1975; Tanzosh & Stone 1995) and is insensitive to detailed form of that force on the spatial scale a. This suggests that the Taylor-column structure would be altered only slightly if the condition $R_o \ll E$ were relaxed. This issue will be explored in a subsequent study.

3.2. *Non-dimensionalization*

In the non-dimensionalization process we shall use the parcel size, a, as the typical length; although the Taylor column is spatially elongated in the direction of the

rotation axis, the fluid within it experiences lateral velocity gradients on the scale of the parcel. Additionally, let

$$\boldsymbol{u}_l = \frac{(\Delta\rho)g}{2\rho\Omega}\boldsymbol{u}^*(\boldsymbol{x}^*), \tag{3.4}$$

$$p = a(\Delta\rho)p^*(\boldsymbol{x}^*) \tag{3.5}$$

and

$$\rho - \rho_0 = -(\Delta\rho)\Psi^*(\boldsymbol{x}^*), \tag{3.6}$$

where an asterisk denotes a dimensionless variable. The problem is viewed from a coordinate system fixed to the buoyant parcel, with $\boldsymbol{x}^*$ measuring distance from the centre of the parcel. The factor $(\Delta\rho)$ is chosen such that $\Psi(\boldsymbol{0}) = 1$. Note that $\boldsymbol{u}^*$ is the velocity of the fluid as seen by an observer fixed to the far fluid, but expressed in coordinates moving with the buoyant parcel; it follows that $\boldsymbol{u}^* \to \boldsymbol{0}$ as $\boldsymbol{x}^* \to \infty$.

Now the dominant-order form of (3.2) is (dropping the asterisks)

$$-\hat{\boldsymbol{\Omega}} \times \boldsymbol{u} + E\nabla_\perp^2 \boldsymbol{u} = \nabla p + \Psi\,\hat{\boldsymbol{g}}, \tag{3.7}$$

where the Ekman number, E, is given by (1.1) and $\nabla_\perp^2 = \nabla^2 - \partial^2/\partial x_\Omega^2$ is the Laplacian in the plane normal to the rotation axis. The inertial terms have been neglected on the basis of assumption (1.3), while the axial viscous term is of smaller order than that retained since $\partial/\partial_\Omega = O(E\partial/\partial x_\perp)$. Note that the upward unit vector $\hat{\boldsymbol{e}}$ used by Moffatt & Loper (1994) is related to $\hat{\boldsymbol{g}}$ by $\hat{\boldsymbol{e}} = -\hat{\boldsymbol{g}}$. Equation (3.7) is equivalent to equation (10′) of that paper.

3.3. *Modal equation and transformation*

Equation (3.3) and (3.7) can be combined into a single *modal equation* for $\boldsymbol{u}$ following the procedure described by Moffatt & Loper (1994). (Take the curl of (3.7) twice and eliminate the vorticity vector between these two equations.) Again neglecting terms of order $E\partial^2/\partial x_\Omega^2$, the result is

$$[E^2\nabla_\perp^6 + (\hat{\boldsymbol{\Omega}}\cdot\nabla)^2]\boldsymbol{u} = -(\hat{\boldsymbol{\Omega}}\cdot\nabla)\hat{\boldsymbol{g}} \times \nabla\Psi + E\nabla_\perp^2\nabla \times [\hat{\boldsymbol{g}} \times \nabla\Psi]. \tag{3.8}$$

This equation is to be solved subject to the condition that the velocity decays to zero at sufficiently large distance from the buoyant parcel. Flow is forced by the terms on the right-hand side of (3.8). Note the baroclinic nature of this forcing; if the density gradient were parallel to gravity, there would be no forcing. The solution has a baroclinic form within the parcel and a geostrophic form outside.

The modal equation is easily solved in Fourier-transform space. Let us introduce the Fourier transform and inverse:

$$\tilde{\boldsymbol{f}}(\boldsymbol{k}) = \int_{\boldsymbol{x}} \boldsymbol{f}(\boldsymbol{x}) \exp(\mathrm{i}\boldsymbol{k}\cdot\boldsymbol{x})\mathrm{d}^3\boldsymbol{x}, \tag{3.9}$$

$$\boldsymbol{f}(\boldsymbol{x}) = \frac{1}{(2\pi)^3}\int_{\boldsymbol{k}} \tilde{\boldsymbol{f}}(\boldsymbol{k}) \exp(-\mathrm{i}\boldsymbol{k}\cdot\boldsymbol{x})\mathrm{d}^3\boldsymbol{k}. \tag{3.10}$$

The Fourier transform of (3.8) yields

$$\tilde{\boldsymbol{u}}(\boldsymbol{k}) = \frac{\boldsymbol{k} \times [(\hat{\boldsymbol{\Omega}}\cdot\boldsymbol{k})\hat{\boldsymbol{g}} + Ek_\perp^2(\boldsymbol{k} \times \hat{\boldsymbol{g}})]}{(\hat{\boldsymbol{\Omega}}\cdot\boldsymbol{k})^2 + E^2k_\perp^6}\,\tilde{\Psi}(\boldsymbol{k}), \tag{3.11}$$

where $k_\perp^2 = \boldsymbol{k}\cdot\boldsymbol{k} - (\hat{\boldsymbol{\Omega}}\cdot\boldsymbol{k})^2$. The Fourier transform was used by Childress (1964) and Tanzosh & Stone (1994) to obtain a Green's function for flow driven by a rigid body,

by Herron *et al.* (1975) to analyse the far-field flow associated with a sedimenting sphere and by Moffatt & Loper (1994) in an analysis of hydromagnetic flow driven by a buoyant parcel. Note that $\tilde{\boldsymbol{u}}(\boldsymbol{k})$ has the same symmetry in $\boldsymbol{k}$, i.e. either odd or even, as $\tilde{\Psi}(\boldsymbol{k})$.

The problem is completed by specification of the buoyancy distribution, which drives the flow. A physically plausible form, which is amenable to mathematical analysis, is the Gaussian distribution employed by Moffatt & Loper (1994); let

$$\Psi(\boldsymbol{x}) = \exp(-x^2), \tag{3.12}$$

where $\boldsymbol{x}$ is the distance from the centre of the buoyant parcel. The Fourier transform of (3.12) is

$$\tilde{\Psi}(\boldsymbol{k}) = \pi^{3/2} \exp(-k^2/4). \tag{3.13}$$

The problem under consideration is linear, so that a more general solution would consist of a sum of buoyant parcels of the form (3.12) with differing magnitudes of density contrast and differing radii. This property provides some generality to the present formulation.

In the following section the velocity vector and associated pressure field are inverted for a general point $\boldsymbol{x}$. The result is summarized in equations (4.20) and (4.21).

4. Fourier inversion

A distinct advantage of the present problem with flow driven by a fluid parcel, as opposed to the problem of flow driven by a rigid body, is that the transform is valid for all space. Consequently no dual integral equations are encountered in the inversion process and the integrals are somewhat easier to evaluate.

4.1. *Velocity field*

Dominant-order contributions to the inversion of (3.11) come from those regions of $\boldsymbol{k}$-space for which $|\tilde{\boldsymbol{u}}| = O(1/\Delta k)$, where Δk is a measure of the size of that region. With $E \ll 1$, there are two such regions. One region, having Δk of unit order, governs the structure of the baroclinic flow on the scale of the buoyant parcel and the second, characterized by $\hat{\boldsymbol{\Omega}} \cdot \hat{\boldsymbol{k}} \ll 1$, governs the geostrophic structure of the Taylor column. In the following analysis, it will be convenient to decompose the wavenumber vector into components parallel and perpendicular to the rotation axis; let

$$\boldsymbol{k} = k_\Omega \hat{\boldsymbol{\Omega}} + \boldsymbol{k}_\perp = k_\Omega \hat{\boldsymbol{\Omega}} + k_\perp \hat{\boldsymbol{k}}_\perp. \tag{4.1}$$

This decomposition of the wavenumber vector introduces a cylindrical coordinate system to guide the inversion integrals. Inversion in the angular direction can be accomplished without approximation; this will be done first. The second inversion in the axial direction can be accomplished to any desired order in powers of E; in what follows each velocity component is correctly expressed at unit order and the radial velocity at order E. The third inversion in the radial direction can be accomplished in closed form within and near the parcel. The resulting inversions will involve a similar cylindrical representation of the position vector:

$$\boldsymbol{x} = x_\Omega \hat{\boldsymbol{\Omega}} + \boldsymbol{x}_\perp = x_\Omega \hat{\boldsymbol{\Omega}} + x_\perp \hat{\boldsymbol{x}}_\perp. \tag{4.2}$$

The Fourier inversions for the angular and axial wavenumbers are presented in

Appendix B. The results may be expressed as

$$\boldsymbol{u}(\boldsymbol{x}) = -\hat{\boldsymbol{g}} \times [V_{s12}(x_\perp, x_\Omega)\hat{\boldsymbol{x}}_\perp + \exp(-x^2)\hat{\boldsymbol{\Omega}}] - \frac{1}{x_\perp} V_{c11}(x_\perp, x_\Omega)[\hat{\boldsymbol{g}} + (\hat{\boldsymbol{g}} \cdot \hat{\boldsymbol{\Omega}})\hat{\boldsymbol{\Omega}}] + [\hat{\boldsymbol{x}}_\perp \times \hat{\boldsymbol{g}}] \times [V_{c22}(x_\perp, x_\Omega)\hat{\boldsymbol{x}}_\perp - E V_{s14}(x_\perp, x_\Omega)\hat{\boldsymbol{\Omega}}], \quad (4.3)$$

where

$$V_{cmn}(x_\perp, x_\Omega) = \frac{\sqrt{\pi}}{4} \int_0^\infty H_c J_m(x_\perp k_\perp) \exp\left(-\frac{k_\perp^2}{4}\right) k_\perp^n \, \mathrm{d}k_\perp, \quad (4.4)$$

$$V_{smn}(x_\perp, x_\Omega) = \frac{\sqrt{\pi}}{4} \int_0^\infty H_s J_m(x_\perp k_\perp) \exp\left(-\frac{k_\perp^2}{4}\right) k_\perp^n \, \mathrm{d}k_\perp, \quad (4.5)$$

$$H_c(k_\perp; x_\Omega) = \cosh(E x_\Omega k_\perp^3) - \mathrm{erf}(x_\Omega) \sinh(E x_\Omega k_\perp^3) \quad (4.6)$$

and

$$H_s(k_\perp; x_\Omega) = \sinh(E x_\Omega k_\perp^3) - \mathrm{erf}(x_\Omega) \cosh(E x_\Omega k_\perp^3). \quad (4.7)$$

For x_Ω of unit order $V_{cmn} > 0$ and the sign of V_{smn} is opposite to that of x_Ω.

Equation (4.3) quantifies the velocity field in terms of a set of four single integrals defined by (4.4) and (4.5). A simpler form of $\boldsymbol{u}(\boldsymbol{x})$ is presented in § 4.3, following solution in § 4.2 for the pressure field.

4.2. *Pressure field*

The dynamic pressure field associated with this solution satisfies

$$\nabla p = -\Psi \hat{\boldsymbol{g}} - \hat{\boldsymbol{\Omega}} \times \boldsymbol{u} + E \nabla_\perp^2 \boldsymbol{u}. \quad (4.8)$$

The viscous term must be kept, as it has a cumulative, dominant-order effect within the Taylor column. Combining the dot product of (4.8) with $\hat{\boldsymbol{\Omega}}$, (4.3), leads to

$$\frac{\partial p}{\partial x_\Omega} = -[E \nabla_\perp^2 V_{c02} + \exp(-x^2)][\hat{\boldsymbol{g}} \cdot \hat{\boldsymbol{\Omega}}] + E \nabla_\perp^2([\hat{\boldsymbol{g}} \times \hat{\boldsymbol{\Omega}} \cdot \hat{\boldsymbol{x}}_\perp] V_{s12}). \quad (4.9)$$

This equation is integrated in Appendix C; the result is

$$p(\boldsymbol{x}) = V_{s01}(x_\perp, x_\Omega)[\hat{\boldsymbol{g}} \cdot \hat{\boldsymbol{\Omega}}] - V_{c11}(x_\perp, x_\Omega)[\hat{\boldsymbol{g}} \times \hat{\boldsymbol{\Omega}} \cdot \hat{\boldsymbol{x}}_\perp]. \quad (4.10)$$

The solution (4.10) has been obtained by integrating the axial component of the momentum equation, which is dominated by the non-geostrophic viscous term. The geostrophic components of (4.8) provide a check on the solution. It is straight-forward but tedious to confirm that solutions (4.3) and (4.10) satisfy the geostrophic equation to dominant order in E.

4.3. *Simplified solutions*

Representations (4.3) and (4.10), quantifying the velocity and pressure fields as functions of position, involve integrals (4.4) and (4.5), the form of which makes them rather difficult to integrate numerically. In this subsection alternative expressions are presented, which are identical at dominant order in powers of E and which are more amenable to numerical evaluation.

Simpler forms of H_c and H_s, equivalent to definitions (4.6) and (4.7) at dominant order, are

$$H_c \approx \exp(-E|x_\Omega|k_\perp^3) \quad (4.11)$$

and

$$H_s = -\mathrm{erf}\,(x_\Omega) H_c. \tag{4.12}$$

Using these, the factors V_{cmn} and V_{smn} which appear in (4.3) and (4.10) may be expressed in simpler form:

$$V_{c11} = \tfrac{1}{4}\pi x_\perp T_1, \tag{4.13}$$

$$V_{c22} = \tfrac{1}{2}\pi(T_1 - S_2), \tag{4.14}$$

$$V_{s01} = -\tfrac{1}{2}\sqrt{\pi}\,\mathrm{erf}\,(x_\Omega) S_1, \tag{4.15}$$

$$V_{s12} = -\sqrt{\pi}\,\mathrm{erf}\,(x_\Omega) x_\perp T_2, \tag{4.16}$$

and

$$V_{s14} = -8\sqrt{\pi}\,\mathrm{erf}\,(x_\Omega) x_\perp T_4, \tag{4.17}$$

where

$$S_n(x_\perp, x_\Omega) = \int_0^\infty \frac{k_\perp^n J_0(x_\perp k_\perp)}{2^n \Gamma[(n+1)/2]} \exp(-E|x_\Omega| k_\perp^3 - \tfrac{1}{4}k_\perp^2)\mathrm{d}k_\perp \tag{4.18}$$

and

$$T_n(x_\perp, x_\Omega) = \int_0^\infty \frac{k_\perp^n J_1(x_\perp k_\perp)}{2^n \Gamma[(n+2)/2] x_\perp} \exp(-E|x_\Omega| k_\perp^3 - \tfrac{1}{4}k_\perp^2)\mathrm{d}k_\perp. \tag{4.19}$$

The integrals S_n and T_n have been normalized such that $S_n(0,0) = T_n(0,0) = 1$. (More precisely, $S_n(x_\perp, 0) \sim 1 - \frac{1}{2}(n+1)x_\perp^2$ and $T_n(x_\perp, 0) \sim 1 - \frac{1}{4}(n+2)x_\perp^2$ for small $x_\perp$.)

Now

$$\begin{aligned}\boldsymbol{u}(\boldsymbol{x}) = -\hat{\boldsymbol{g}} \times [\sqrt{\pi}\,\mathrm{erf}\,(x_\Omega) T_2(x_\perp, x_\Omega)\boldsymbol{x}_\perp - \exp(-x^2)\hat{\boldsymbol{\Omega}}] - \tfrac{1}{4}\pi T_1(x_\perp, x_\Omega)[\hat{\boldsymbol{g}} + (\hat{\boldsymbol{g}} \cdot \hat{\boldsymbol{\Omega}})\hat{\boldsymbol{\Omega}}] \\ + [\hat{\boldsymbol{x}}_\perp \times \hat{\boldsymbol{g}}] \times \left\{ \frac{\pi}{2} \left[\frac{T_1(x_\perp, x_\Omega) - S_2(x_\perp, x_\Omega)}{x_\perp^2} \right] \boldsymbol{x}_\perp + 8\sqrt{\pi} E\,\mathrm{erf}\,(x_\Omega) T_4(x_\perp, x_\Omega)\hat{\boldsymbol{\Omega}} \right\}\end{aligned} \tag{4.20}$$

and

$$p(\boldsymbol{x}) = -\tfrac{1}{2}\sqrt{\pi}\,\mathrm{erf}\,(x_\Omega) S_1(x_\perp, x_\Omega)[\hat{\boldsymbol{g}} \cdot \hat{\boldsymbol{\Omega}}] + \tfrac{1}{4}\pi T_1(x_\perp, x_\Omega)[\hat{\boldsymbol{\Omega}} \times \hat{\boldsymbol{g}} \cdot \boldsymbol{x}_\perp]. \tag{4.21}$$

Note the change from $\hat{\boldsymbol{x}}_\perp$ to $\boldsymbol{x}_\perp$.

4.4. *Gravity and rotation antiparallel*

In the case that $\boldsymbol{g}$ and $\boldsymbol{\Omega}$ are antiparallel (4.20) and (4.21) simplify to

$$\begin{aligned}\boldsymbol{u}(\boldsymbol{x}) = \tfrac{1}{2}\pi S_2(x_\perp, x_\Omega)\hat{\boldsymbol{\Omega}} + 8\sqrt{\pi} E\,\mathrm{erf}\,(x_\Omega) T_4(x_\perp, x_\Omega)\boldsymbol{x}_\perp \\ -\sqrt{\pi}\,\mathrm{erf}\,(x_\Omega) T_2(x_\perp, x_\Omega)[\hat{\boldsymbol{\Omega}} \times \boldsymbol{x}_\perp]\end{aligned} \tag{4.22}$$

and

$$p(\boldsymbol{x}) = \tfrac{1}{2}\sqrt{\pi}\,\mathrm{erf}\,(x_\Omega) S_1(x_\perp, x_\Omega). \tag{4.23}$$

The first and second terms on the right-hand side of (4.22) represent an axisymmetric meridional flow. The stream function for this flow (as defined by Batchelor 1967, eqn (2.2.11)) is

$$\psi(\boldsymbol{x}) = \tfrac{1}{4}\pi x_\perp^2 T_1(x_\perp, x_\Omega). \tag{4.24}$$

Isolines of the stream function are plotted on a meridional cross-section in figures 2(*a*) and 2(*b*). Note that these cross-sections are on the Taylor-column scale. On this scale the fluid parcel has no finite axial extent and lies on the horizontal axis of the

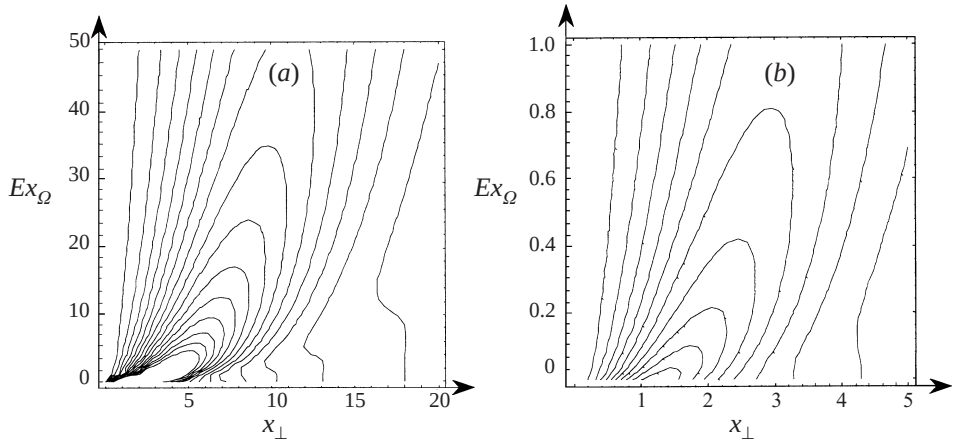

FIGURE 2. (a, b) Isoline plots of the stream function in the antiparallel case depicted on a meridional cross-section.

figures. The figures are symmetric about the equatorial plane of the parcel; the lower half is not shown. Note the similarity of the isolines of figure 2(a) to those depicted in figure 3(a) of Tanzosh & Stone (1994).

Flow is parallel to the isolines. Where the isolines are horizontal, the axial velocity component is zero and where vertical, the radial velocity is zero. Fluid near the symmetry axis lying above the parcel, satisfying $x_\perp < Y(x_\Omega)$, moves upward and (weakly) radially outward, while fluid farther out, satisfying $Y(x_\Omega) < x_\perp$, moves downward and alternately outward and inward as $x_\perp$ increases. The first alternation in sign of radial velocity component is evident in figure 2(a, b). The function $Y(x_\Omega)$ is found by solving the implicit equation $S_2(x_\perp, x_\Omega) = 0$, that is,

$$\int_0^\infty k_\perp^2 J_0(x_\perp k_\perp) \exp(-E|x_\Omega|k_\perp^3 - \tfrac{1}{4}k_\perp^2)\mathrm{d}k_\perp = 0. \tag{4.25}$$

The function $Y(x_\Omega)$ is graphed in figure 3. This displays a physical meridional cross-section on the scale of the Taylor column. On this scale the fluid parcel has no finite axial extent and lies on the horizontal axis of the figure. The figure is symmetric about the equatorial plane of the parcel; the lower half is not shown. This graph of $x_\perp = Y(x_\Omega)$ does not intercept the $x_\perp$-axis vertically on the Taylor-column scale depicted in figure 3; on the scale of the parcel, the flow structure is axially invariant at dominant order. As $x_\perp$ becomes large, the curve asymptotes to $0.0386613x_\perp^3$.

The third term of equation (4.22) describes a swirl that is retrograde ahead of the parcel and prograde behind. This swirl is in geostrophic balance with the pressure given by (4.23). The swirl and pressure are antisymmetric about the equatorial plane of the parcel (i.e. the plane defined by $x_\Omega = 0$) and have structure on both the scale of the parcel, quantified by the error function, and on the scale of the Taylor column, quantified the functions S_n and T_n. Isolines of the swirl angular velocity, $u_s/x_\perp$, and pressure are quantified by

$$u_s(\boldsymbol{x})/x_\perp = -\sqrt{\pi}\, T_2(x_\perp, x_\Omega)/x_\perp \tag{4.26}$$

and (4.23). Formula (4.26) is valid provided x_Ω is positive and much larger than unity; if $x_\Omega < 0$ the swirl velocity has the opposite sign. Isolines of $u_s/x_\perp$ and p are plotted in figures 4(a) and 4(b). The similarity between the two is due to the geostrophic balance in the Taylor column, between the swirl angular velocity and the gradient

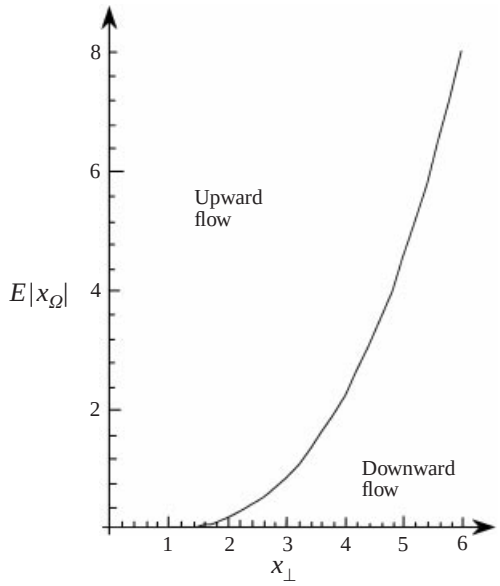

FIGURE 3. Depiction of regions of upward flow and counter flow on the meridional plane at the Taylor-column scale in the antiparallel case.

of the pressure. A comparable plot of the swirl driven by a point force is given in figure 3(*b*) of Tanzosh & Stone (1994). The swirl produced by a spatially extended fluid parcel is significantly larger than that produced by a point force. The differences between these two representations are due to two factors. First, the dominant balance near the point force is Stokesian rather than geostrophic and the source producing the isolines of figure 4(*a*) is of finite horizontal extent. On the scale of this figure the buoyant parcel has an infinitesimal axial extent. The swirl angular velocity and pressure are each a maximum on the symmetry axis adjacent to the fluid parcel, i.e. at the origin in figure 4(*a*, *b*).

Outside the parcel, the pressure distribution given by (4.23) integrates to give a force

$$F_P = 2\pi \int_0^\infty p(\boldsymbol{x}) x_\perp \, \mathrm{d}x_\perp = \operatorname{sgn}(x_\Omega)\pi^{3/2} \int_0^\infty S_1(x_\perp, x_\Omega) x_\perp \, \mathrm{d}x_\perp, \tag{4.27}$$

pointing opposite to gravity. This force exactly balances the buoyancy force of the parcel provided

$$\int_0^\infty S_1(x_\perp, x_\Omega) x_\perp \, \mathrm{d}x_\perp = \tfrac{1}{2}. \tag{4.28}$$

The validity of this condition may be demonstrated as follows. Eliminate S_1 with (4.18), use the identity $zJ_0(z) = \mathrm{d}[zJ_1(z)]/\mathrm{d}z$ and then integrate by parts over $k_\perp$. Next interchange the order of integration and integrate over $x_\perp$ and $k_\perp$ in turn.

4.5. *Gravity and rotation perpendicular*

In the case the $\boldsymbol{g}$ and $\boldsymbol{\Omega}$ are perpendicular, solutions (4.20) and (4.21) simplify to

$$\begin{aligned} \boldsymbol{u}(\boldsymbol{x}) = \hat{\boldsymbol{g}} \times [\sqrt{\pi} \operatorname{erf}(x_\Omega) T_2(x_\perp, x_\Omega) \boldsymbol{x}_\perp - \exp(-x^2) \hat{\boldsymbol{\Omega}}] \\ - \frac{\pi}{4} T_1(x_\perp, x_\Omega) \hat{\boldsymbol{g}} + \frac{\pi}{2} \left[\frac{S_2(x_\perp, x_\Omega) - T_1(x_\perp, x_\Omega)}{x_\perp^2} \right] \boldsymbol{x}_\perp \times [\boldsymbol{x}_\perp \times \hat{\boldsymbol{g}}] \end{aligned} \tag{4.29}$$

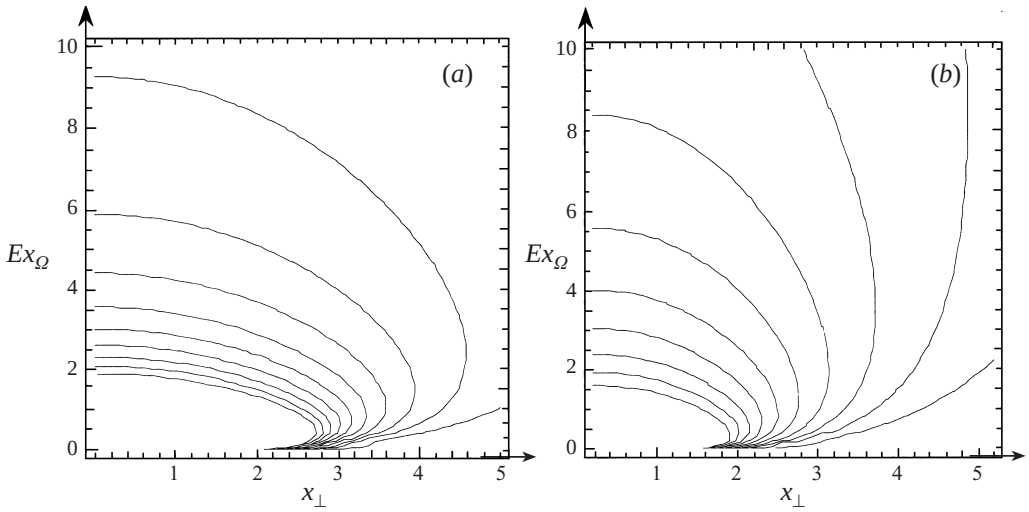

FIGURE 4. Isolines of (*a*) the swirl angular velocity and (*b*) pressure for the case when rotation and gravity are aligned.

and

$$p(\boldsymbol{x}) = -\tfrac{1}{4}\pi[\hat{\boldsymbol{g}} \times \hat{\boldsymbol{\Omega}} \cdot \boldsymbol{x}_\perp] T_1(x_\perp, x_\Omega). \tag{4.30}$$

The flow in this case is more complicated than in the antiparallel case of § 4.4, now being a function of all three spatial coordinates, and is not easily summarized graphically. Rather than attempting a graph for this special case, attention will now be returned to the general case.

Although the integrals S_n and T_n cannot be evaluated in closed form for all values of x_Ω and $x_\perp$, the behaviour in several regions of physical space is relatively simple and illuminating. This behaviour is investigated in the following three sections. Specifically the velocity and pressure along the modal axis (i.e. where $x_\perp = 0$) are discussed in § 5, far from the parcel in the direction of the Taylor column (i.e. where $E|x_\Omega| \gg 1$) are investigated in § 6 and in the vicinity of the parcel (where $E|x_\Omega| \ll 1$) are studied in § 7.

5. Velocity and pressure at the origin and on the modal axis

Since the integrals S_n and T_n have been normalized, the velocity at the origin for general orientation of gravity and rotation is easily evaluated; (4.20) yields

$$\boldsymbol{u}(0) = -\tfrac{1}{4}\pi[\hat{\boldsymbol{g}} + (\hat{\boldsymbol{g}} \cdot \hat{\boldsymbol{\Omega}})\hat{\boldsymbol{\Omega}}] + \hat{\boldsymbol{\Omega}} \times \hat{\boldsymbol{g}}. \tag{5.1}$$

This dimensionless velocity is identical to the dimensional version given in equation (2.8). The latter was found by Moffatt & Loper (1994) for a parcel in a rotating hydromagnetic fluid. However, as we shall see in § 8, this is not the rise velocity of the parcel as Moffatt & Loper had assumed.

The modal axis is that line in space parallel to the axis of rotation, having $x_\perp = 0$. On that axis, solutions (4.20) and (4.21) simplify to

$$\boldsymbol{u}(x_\Omega \hat{\boldsymbol{\Omega}}) = [\hat{\boldsymbol{\Omega}} \times \hat{\boldsymbol{g}}] \exp(-x_\Omega^2) - [\hat{\boldsymbol{g}} + (\hat{\boldsymbol{g}} \cdot \hat{\boldsymbol{\Omega}})\hat{\boldsymbol{\Omega}}] U(x_\Omega) \tag{5.2}$$

and

$$p(x_\Omega \hat{\boldsymbol{\Omega}}) = -[\hat{\boldsymbol{g}} \cdot \hat{\boldsymbol{\Omega}}] \operatorname{erf}(x_\Omega) P(x_\Omega), \tag{5.3}$$

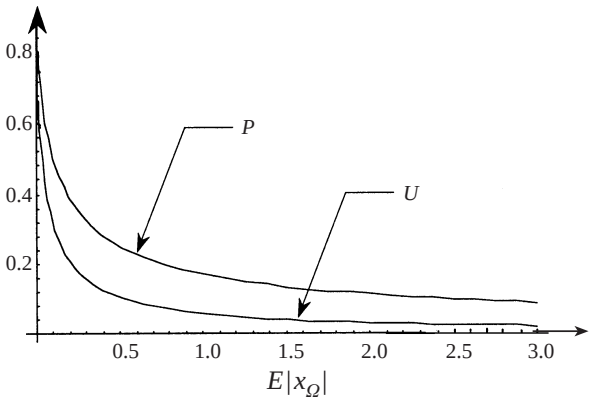

FIGURE 5. Graphs of U and P versus $E|x_\Omega|$.

where

$$U(x_\Omega) = \frac{\sqrt{\pi}}{8} \int_0^\infty k_\perp^2 \exp(-E|x_\Omega|k_\perp^3 - \tfrac{1}{4}k_\perp^2)\, \mathrm{d}k_\perp \tag{5.4}$$

and

$$P(x_\Omega) = \frac{\sqrt{\pi}}{4} \int_0^\infty k_\perp^2 \exp(-E|x_\Omega|k_\perp^3 - \tfrac{1}{4}k_\perp^2)\, \mathrm{d}k_\perp. \tag{5.5}$$

Note that $U(0) = \pi/4$ and $P(0) = \sqrt{\pi}/2$.

The velocity on the modal axis is symmetric about the equatorial plane of the parcel, while the pressure is antisymmetric. The velocity and pressure have variations on both the scale of the parcel (quantified by the error function) and the scale of the Taylor column (quantified by U and P). In the vicinity of the parcel they behave as

$$\boldsymbol{u}(x_\Omega \hat{\boldsymbol{\Omega}}) = [\hat{\boldsymbol{\Omega}} \times \hat{\boldsymbol{g}}] \exp(-x_\Omega^2) - \frac{\pi}{4}[\hat{\boldsymbol{g}} + (\hat{\boldsymbol{g}} \cdot \hat{\boldsymbol{\Omega}})\hat{\boldsymbol{\Omega}}] \tag{5.6}$$

and

$$p(x_\Omega \hat{\boldsymbol{\Omega}}) = -\frac{\sqrt{\pi}}{2}[\hat{\boldsymbol{g}} \cdot \hat{\boldsymbol{\Omega}}] \operatorname{erf}(x_\Omega). \tag{5.7}$$

Outside the parcel (i.e. where $|x_\Omega| \gg 1$) the velocity and pressure are

$$\boldsymbol{u}(x_\Omega \hat{\boldsymbol{\Omega}}) = -U(x_\Omega)[\hat{\boldsymbol{g}} + (\hat{\boldsymbol{g}} \cdot \hat{\boldsymbol{\Omega}})\hat{\boldsymbol{\Omega}}] \tag{5.8}$$

and

$$p(x_\Omega \hat{\boldsymbol{\Omega}}) = -[\hat{\boldsymbol{g}} \cdot \hat{\boldsymbol{\Omega}}] \operatorname{sgn}(x_\Omega) P(x_\Omega). \tag{5.9}$$

Note that in the antiparallel case, the speed at the origin is $2U$.

The variations of functions $U(x_\Omega)$ and $P(x_\Omega)$ with axial distance are shown in figure 5. Note that the horizontal axis of this figure depicts the Taylor-column scale, which is a very large axial distance when measured by the scale of the parcel. It is seen that the velocity and pressure initially decrease rapidly with axial distance. Specifically, when $E|x_\Omega| \ll 1$,

$$U \approx \tfrac{1}{4}\pi - 8\sqrt{\pi}E|x_\Omega| \approx 0.785398 - 14.1796E|x_\Omega| \tag{5.10}$$

and

$$P \approx \tfrac{1}{2}\sqrt{\pi} - 3\pi E|x_\Omega| \approx 0.886227 - 9.42476E|x_\Omega|. \tag{5.11}$$

Experimental studies of the structure of a Taylor column (Taylor 1922; Pritchard

1969; Maxworthy 1970) find that a 'Taylor slug' of fluid moves with the rigid body generating the column. The existence of this slug of recirculating fluid has been confirmed theoretically by Vedensky & Ungarish (1994) for axial flow of a circular disk and by Tanzosh & Stone (1994) for axial flow of a sphere. In fact, the former authors defined the axial extent of the Taylor column by the location of the upper stagnation point. It is clear from figure 5 that no such region exists in a Taylor column produced by a buoyant parcel. It is shown in § 7 that flow driven by axial motion of a fluid parcel is non-uniform; the axial flow diminishes with distance from the symmetry axis. It is likely that this flow structure serves to 'streamline' the parcel and allow the fluid in the Taylor column to move radially outward then axially backward relative to the parcel in a smooth fashion. This smoothing is evident in the fact that the buoyant parcel does not produce any singularity, such as that which occurs at the circumference of a circular disk (Vedensky & Ungarish 1994).

Maxworthy (1970) found that the Taylor slug is typically $O(0.1a/E)$ in axial extent and the result of Vedensky & Ungarish (1994) is in general agreement with this observation; they located the upper stagnation point at a distance $0.051/E$ from the disk. Figure 5 and (5.10) are in rough agreement with these observations; the axial velocity decays rapidly with distance from the body, reaching 50% of its maximum value roughly at $E|x_\Omega| \approx 0.1$. However, note that there is a long tail extending fore and aft of the parcel; the velocity and pressure decay algebraically with axial distance:

$$U(x_\Omega) \approx \frac{\sqrt{\pi}}{24E|x_\Omega|} \approx \frac{0.073852}{E|x_\Omega|} \tag{5.12}$$

and

$$P(x_\Omega) \approx \frac{\pi\Gamma(5/6)}{6(2)^{1/3}(3)^{1/2}\Gamma(2/3)(E|x_\Omega|)^{2/3}} \approx \frac{0.20001}{(E|x_\Omega|)^{2/3}}. \tag{5.13}$$

An algebraic decay of pressure is necessary if it is to balance buoyancy at all axial positions; see (4.27) and (4.28).

6. Velocity and pressure far from the parcel

In this section expressions (4.20) and (4.21) for the velocity and pressure are evaluated sufficiently far from the parcel that $E|x_\Omega| \gg 1$. In this limit, dominant-order contributions to the integrals defined by (4.18) and (4.19) occur where $k_\perp \ll 1$. It follows that the factor $k_\perp^2/4$ in the exponentials of these integrals may be ignored. Physically this implies that the far-field behaviour is independent of the structure of the buoyant parcel, and is sensitive only to the total buoyancy. It follows that the results of this section are expected to be valid for fluid parcels having a shape other than Gaussian and for solid bodies having the same total buoyancy as the Gaussian parcel.

In this limit the integrals S_n and T_n, which are in general functions of two variables, x_Ω and $x_\perp$, may be expressed in terms of integrals involving a single similarity variable,

$$\xi = x_\perp/(E|x_\Omega|)^{1/3}. \tag{6.1}$$

Note the occurrence of the $1/3$ power in this variable; the asymptotic structure of the Taylor column is determined by the same dynamical balance as Stewartson's $E^{1/3}$ sidewall layer (Stewartson 1957). In a closed container having $x_\Omega = O(1)$, ξ is of unit order when $x_\perp = O(E^{1/3})$; this is the structure of a Stewartson layer. In the present case, both x_Ω and $x_\perp$ are large, but with $\xi = O(1)$. Now (4.18) and (4.19) may be

expressed as

$$S_n(x_\perp, x_\Omega) = \frac{\Gamma[(n+1)/3]}{3(2^n)\Gamma[(n+1)/2](E|x_\Omega|)^{(n+1)/3}} s_n(\xi) \tag{6.2}$$

and

$$T_n(x_\perp, x_\Omega) = \frac{\Gamma[(n+2)/3]}{2^{n+1}\,3\Gamma[(n+2)/2](E|x_\Omega|)^{(n+2)/3}} t_n(\xi), \tag{6.3}$$

where

$$s_n(\xi) = \int_0^\infty \frac{3q^n J_0(\xi q)}{\Gamma[(n+1)/3]} \exp(-q^3)\,\mathrm{d}q \tag{6.4}$$

and

$$t_n(\xi) = \int_0^\infty \frac{6q^n J_1(\xi q)}{\Gamma[(n+2)/3]\xi} \exp(-q^3)\,\mathrm{d}q. \tag{6.5}$$

The functions $s_n(\xi)$ and $t_n(\xi)$ have been normalized so that $s_n(0) = t_n(0) = 1$. The asymptotic behaviour of these integrals can be determined by expressing the Bessel functions J_0 and J_1 in terms of the modified Bessel functions, K_0 and K_1, then starting the integration along the imaginary q-axis. The results of interest are

$$s_1(\xi) \sim -\frac{27}{\Gamma[2/3]}\frac{1}{\xi^5}, \tag{6.6}$$

$$s_2(\xi) \sim -3/\xi^3, \tag{6.7}$$

$$t_1(\xi) \sim 6/\xi^3, \tag{6.8}$$

$$t_2(\xi) \sim -\frac{270}{\Gamma[4/3]}\frac{1}{\xi^7}, \tag{6.9}$$

and

$$t_4(\xi) \sim 9450/\xi^9. \tag{6.10}$$

Numerical comparisons using *Mathematica* reveal that these asymptotic formulas should be used in place of (6.4) and (6.5) when $\xi > 15$.

Substitution of (6.2) and (6.3) into (4.20) and (4.21) yields

$$\begin{aligned}\boldsymbol{u}(\boldsymbol{x}) \sim\ & -\frac{\sqrt{\pi}}{24E|x_\Omega|} t_1(\xi)[\hat{\boldsymbol{g}} + (\hat{\boldsymbol{g}}\cdot\hat{\boldsymbol{\Omega}})\hat{\boldsymbol{\Omega}}] + \operatorname{sgn}(x_\Omega)\frac{\Gamma[4/3]\sqrt{\pi}}{24E|x_\Omega|}\xi t_2(\xi)(\hat{\boldsymbol{g}}\times\hat{\boldsymbol{x}}_\perp) \\ & + \frac{\sqrt{\pi}}{12E|x_\Omega|}[s_2(\xi) - t_1(\xi)]\hat{\boldsymbol{x}}_\perp \times (\hat{\boldsymbol{x}}_\perp \times \hat{\boldsymbol{g}}) \\ & - \operatorname{sgn}(x_\Omega)\frac{\sqrt{\pi}E}{24(E|x_\Omega|)^2}\xi t_4(\xi)\hat{\boldsymbol{\Omega}} \times (\hat{\boldsymbol{x}}_\perp \times \hat{\boldsymbol{g}})\end{aligned} \tag{6.11}$$

and

$$p(\boldsymbol{x}) \sim -\frac{\sqrt{\pi}}{24(E|x_\Omega|)^{2/3}}[\operatorname{sgn}(x_\Omega)2\Gamma(\tfrac{2}{3})[\hat{\boldsymbol{g}}\cdot\hat{\boldsymbol{\Omega}}]s_1(\xi) + [\hat{\boldsymbol{g}}\times\hat{\boldsymbol{\Omega}}\cdot\hat{\boldsymbol{x}}_\perp]\xi t_1(\xi)]. \tag{6.12}$$

Each of the terms in (6.11) and (6.12) is a function of the similarity variable ξ divided by a power of $E|x_\Omega|$, indicating an algebraic decay in the axial direction. This far-field flow is geostrophic; $|\boldsymbol{u}|^{-1}|\,\mathrm{d}\boldsymbol{u}/\mathrm{d}x_\Omega| = O(E)$ and $p^{-1}\,\mathrm{d}p/\mathrm{d}x_\Omega = O(E)$.

6.1. *Gravity and rotation antiparallel*

This far-field solution can best be understood in the antiparallel case; now (6.11) and (6.12) simplify to

$$\boldsymbol{u}(\boldsymbol{x}) \sim \frac{\sqrt{\pi}\, s_2(\xi)}{12E|x_\Omega|}\hat{\boldsymbol{\Omega}} + \operatorname{sgn}(x_\Omega)\frac{\sqrt{\pi}}{24E^2 x_\Omega^2} t_4(\xi)\hat{\boldsymbol{x}}_\perp - \operatorname{sgn}(x_\Omega)\frac{\sqrt{\pi}\,\Gamma(1/3)}{12E|x_\Omega|}\xi t_2(\xi)(\hat{\boldsymbol{\Omega}} \times \hat{\boldsymbol{x}}_\perp) \tag{6.13}$$

and

$$p(\boldsymbol{x}) \sim -\operatorname{sgn}(x_\Omega)\frac{\Gamma[2/3]\sqrt{\pi}}{12(E|x_\Omega|)^{2/3}} s_1(\xi). \tag{6.14}$$

The structures of the components of the velocity field and the pressure as functions of ξ are quantified in figure 6.

The first term on the right-hand side of (6.13) represents vertical motion within the Taylor column and the second represents the associated small radial flow. These functions are plotted versus ξ in figures 6(*a*) and 6(*b*). The axial velocity decays as ξ^{-3} while the radial velocity decays as ξ^{-9}. The stream function for this flow may be expressed as

$$\psi(\boldsymbol{x}) = \frac{\sqrt{\pi}\xi^2 t_1(\xi)}{24(E|x_\Omega|)^{1/3}} = \frac{\sqrt{\pi}x_\perp^2 t_1(\xi)}{24E|x_\Omega|}. \tag{6.15}$$

This function is plotted versus ξ in figure 6(*c*). Note that the stream function decays slowly with both increasing axial distance and increasing similarity variable: as $|x_\Omega|^{-1/3}$ and ξ^{-1}.

A co-axial swirl, which develops due to the radial motion, is represented by the third term on the right-hand side of (6.13) and plotted versus ξ in figure 6(*d*). The swirl is retrograde ahead of the parcel and prograde behind. The pressure field associated with this swirl is quantified by (6.14) and plotted versus ξ in figure 6(*e*).

On the modal axis (i.e. where $\xi = 0$), (6.13) yields an axial speed which varies as $\sqrt{\pi}/12E|x_\Omega|$ at large distances, which is in agreement with (5.8) and (5.12). It may be seen from figure 6(*b*) that the axial speed is zero when $\xi \approx 2.957$. This quantifies the asymptotic behaviour of the curve graphed in figure 3. Fluid in the region satisfying $x_\perp < 2.957(E|x_\Omega|)^{1/3}$ is moving in the same direction as the parcel while fluid in the region satisfying $x_\perp > 2.957(E|x_\Omega|)^{1/3}$ is moving oppositely.

6.2. *Gravity and rotation orthogonal*

In this case the solution can be compared with the asymptotic flow produced by the translation of a rigid sphere found by Herron *et al.* (1975). Although that analysis was limited to small Taylor number T_a, the asymptotic structure of the outer flow field at order $T_a^{1/2}$ is identical to that for large Taylor number considered here. Specifically equations (2.23*a*, *b*, *c*) of Herron *et al.* may be compared with the first three terms of (6.6) with gravity and rotation assumed orthogonal.

That outer flow field is associated with motion in the negative $\boldsymbol{h}_1$-direction. At small Taylor number, the drag is parallel to the motion; a force must be applied to the sphere in the negative $\boldsymbol{h}_1$-direction. In the present case flow is driven by a buoyancy force in the direction opposite to gravity (provided $\Delta\rho > 0$). It follows that we may associate $\{\boldsymbol{h}_1, \boldsymbol{h}_2, \boldsymbol{h}_3\}$ with $\{\hat{\boldsymbol{g}}, \hat{\boldsymbol{\Omega}} \times \hat{\boldsymbol{g}}, \hat{\boldsymbol{\Omega}}\}$ and write

$$\boldsymbol{u}(\boldsymbol{x}) = u'\hat{\boldsymbol{g}} + v'(\hat{\boldsymbol{\Omega}} \times \hat{\boldsymbol{g}}) + w'\hat{\boldsymbol{\Omega}}, \tag{6.16}$$

with the velocity components having the same physical meaning as those employed

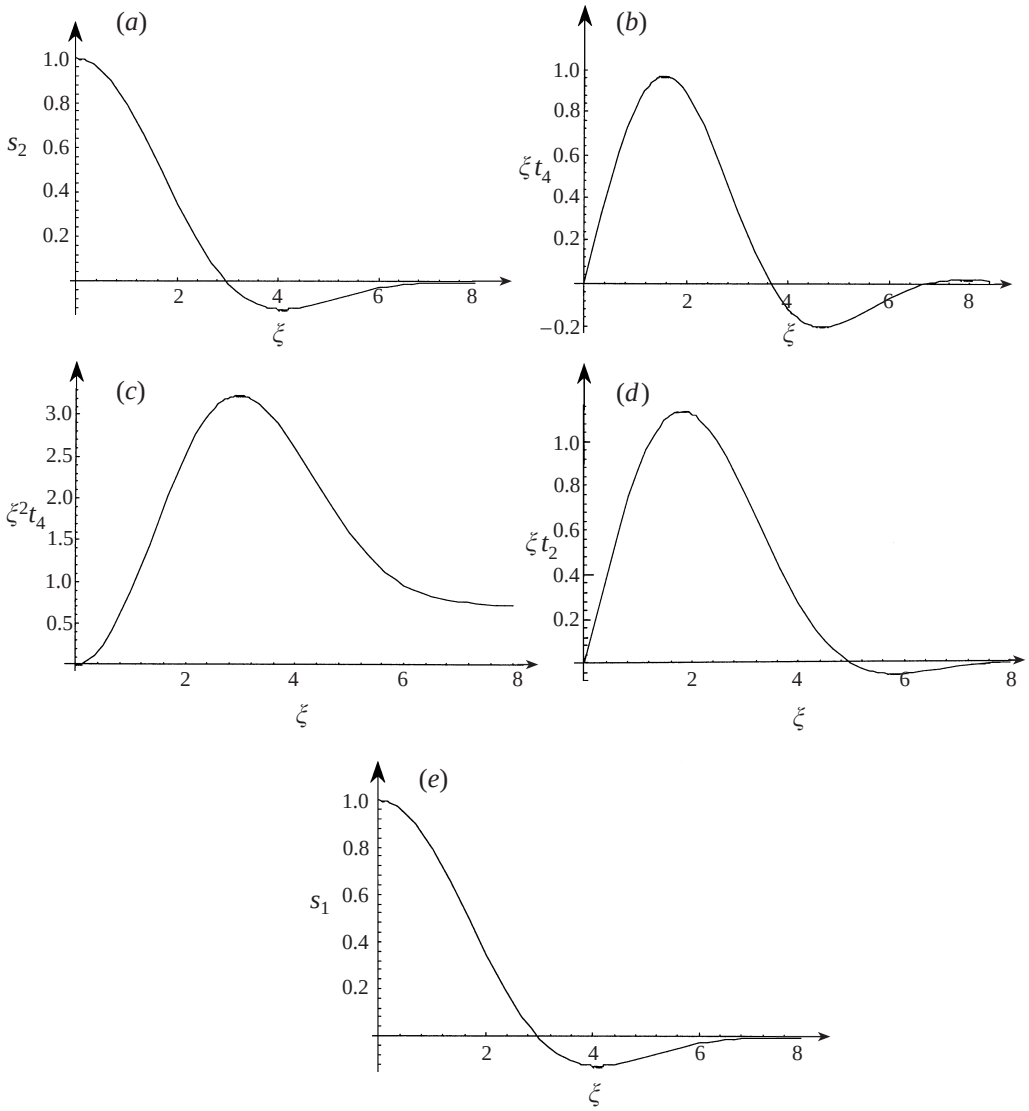

FIGURE 6. Plots of the normalized (*a*) axial velocity, (*b*) radial velocity, (*c*) stream function, (*d*) swirl velocity and (*e*) far pressure field as a function of the similarity variable in the case that rotation and gravity are co-linear.

by Herron *et al.* (1975). Using (6.16) and noting that α is the angle between $\hat{\boldsymbol{x}}_\perp$ and $\hat{\boldsymbol{g}}$, (6.11) may be written as

$$u' \sim -\frac{\sqrt{\pi}}{24E|x_\Omega|}\{s_2(\xi) + [s_2(\xi) - t_1(\xi)]\cos(2\alpha)\}, \tag{6.17}$$

$$v' \sim \frac{\sqrt{\pi}\sin(2\alpha)}{24E|x_\Omega|}[s_2(\xi) - t_1(\xi)], \tag{6.18}$$

$$w' \sim \frac{\Gamma[1/3]\sqrt{\pi}\cos(\alpha)}{72Ex_\Omega}\xi t_2(\xi), \tag{6.19}$$

for the fluid parcel. Noting that

$$\int_0^\infty q^2 J_0(\xi q)\exp(-q^3)\,\mathrm{d}q = \tfrac{1}{3}s_2(\xi), \tag{6.20}$$

$$\int_0^\infty q^2 J_1(\xi q)\exp(-q^3)\,\mathrm{d}q = \tfrac{1}{18}\Gamma(1/3)\xi t_2(\xi), \tag{6.21}$$

$$\int_0^\infty q^2 J_2(\xi q)\exp(-q^3)\,\mathrm{d}q = \tfrac{1}{3}[t_1(\xi) - s_2(\xi)], \tag{6.22}$$

equations (2.23a,b,c) of Herron *et al.* may be expressed as

$$u' \sim -\frac{1}{4|z'|}\{s_2(\xi) + [s_2(\xi) - t_1(\xi)]\cos(2\alpha)\}, \tag{6.23}$$

$$v' \sim \frac{\sin(2\alpha)}{4|z'|}[s_2(\xi) - t_1(\xi)], \tag{6.24}$$

$$w' \sim \frac{\Gamma[1/3]\cos(\alpha)}{12z'}\xi t_2(\xi). \tag{6.25}$$

It is readily apparent that the two solutions have the same structure. The amplitudes are identical as well provided that z' is associated with $6Ex_\Omega/\sqrt{\pi}$. This provides a valuable check on the validity and accuracy of the present solution.

7. Velocity and pressure fields close to the parcel

If $E|x_\Omega| \ll 1$, then the terms in the integrals defined by (4.18) and (4.19) involving this factor are negligibly small. The simplified integrals may be evaluated using Watson (1966 formulas 13.3(4) and (5), p. 394 with $\nu = 0, 1$, $a = x_\perp$, $p^2 = 1/4$, plus their derivatives). The dominant-order results may be expressed compactly as

$$\boldsymbol{u}(\boldsymbol{x}) = \hat{\boldsymbol{g}} \times \nabla\Phi(x_\perp, x_\Omega) + \hat{\boldsymbol{\Omega}} \times \nabla\Psi(\boldsymbol{x}_\perp) + [\pi/4]\nabla^2 f_0(x_\perp)[\hat{\boldsymbol{g}} \cdot \hat{\boldsymbol{\Omega}}]\hat{\boldsymbol{\Omega}} \tag{7.1}$$

and

$$p(\boldsymbol{x}) = [\hat{\boldsymbol{g}} \cdot \hat{\boldsymbol{\Omega}}]\Phi(x_\perp, x_\Omega) + \Psi(\boldsymbol{x}_\perp), \tag{7.2}$$

where

$$\Phi[x_\perp, x_\Omega] = -[\sqrt{\pi}/2]\,\mathrm{erf}(x_\Omega)\exp(-x_\perp^2), \tag{7.3}$$

$$\Psi(\boldsymbol{x}_\perp) = (\pi/4)[f_1(x_\perp) - f_0(x_\perp)]\hat{\boldsymbol{g}} \times \hat{\boldsymbol{\Omega}} \cdot \boldsymbol{x}_\perp, \tag{7.4}$$

and

$$f_n(x_\perp) = \exp(-x_\perp^2/2)I_n(x_\perp^2/2). \tag{7.5}$$

Here I_n is a modified Bessel function. Note that (7.1)–(7.5) represents a *complete analytic solution* of the flow and pressure in the vicinity of the buoyant parcel.

A more explicit and useful representation of the solution is

$$\begin{aligned}\boldsymbol{u}(\boldsymbol{x}) = {} & -\tfrac{1}{4}\pi[f_0(x_\perp) - f_1(x_\perp)][\hat{\boldsymbol{g}} + (\hat{\boldsymbol{g}} \cdot \hat{\boldsymbol{\Omega}})\hat{\boldsymbol{\Omega}}] + \sqrt{\pi}\,\mathrm{erf}(x_\Omega)\exp(-x_\perp^2)(\hat{\boldsymbol{g}} \times \boldsymbol{x}_\perp) \\ & + \exp(-x^2)(\hat{\boldsymbol{\Omega}} \times \hat{\boldsymbol{g}}) + \frac{\pi}{2}\left[f_0(x_\perp) - \left(1 + \frac{1}{x_\perp^2}\right)f_1(x_\perp)\right]\boldsymbol{x}_\perp \times (\hat{\boldsymbol{g}} \times \boldsymbol{x}_\perp)\end{aligned} \tag{7.6}$$

and

$$p(\boldsymbol{x}) = -\tfrac{1}{2}\sqrt{\pi}[\hat{\boldsymbol{g}} \cdot \hat{\boldsymbol{\Omega}}]\,\mathrm{erf}(x_\Omega)\exp(-x_\perp^2) - \tfrac{1}{4}\pi[\hat{\boldsymbol{g}} \times \hat{\boldsymbol{\Omega}} \cdot \boldsymbol{x}_\perp][f_0(x_\perp) - f_1(x_\perp)]. \tag{7.7}$$

The velocity and pressure within the domain of the buoyant parcel satisfy a baroclinic balance, while outside the parcel the balance is geostrophic. On the scale considered in this section, this geostrophic balance is axially invariant, in accordance with Taylor's theorem. The fluid flow in the vicinity of the parcel, quantified by the four terms on the right-hand side of (7.6), respectively consists of:

(i) a geostrophic motion in the direction of rise (having an area average identically zero) which decays algebraically (as $1/x_\perp^3$) in the radial direction;

(ii) a swirl normal to the gravity vector decaying exponentially in the radial direction, which is baroclinic within the domain of the parcel (behaving as the error function in the axial direction) and geostrophic outside;

(iii) a baroclinic out-of-plane motion confined to the domain of the buoyant parcel (i.e. decaying exponentially in the radial and axial directions);

(iv) an azimuthally modulated geostrophic motion, which is zero on the modal axis and decays algebraically (as $1/x_\perp^3$) in the radial direction. This motion is zero on the modal axis, so that it does not contribute to the rise velocity. It acts to change the cross-sectional shape of the parcel from circular to elliptic.

The structure of the pressure field is somewhat simpler than that of the velocity field, consisting of the two terms on the right-hand side of (7.7):

(i) a pressure that is radially confined to the domain of the parcel, and antisymmetric in the axial direction. The pressure force associated with this term is responsible for balancing the buoyancy force and swirl within the parcel and balancing the swirl outside the parcel, within the Taylor column;

(ii) an azimuthally modulated pressure that decays algebraically (as $1/x_\perp^2$) in the radial direction and is symmetric in the axial direction. The gradient of this pressure balances the modulated geostrophic motion.

The velocity at the centre of the parcel may be obtained by setting $x_\Omega = x_\perp = 0$ in (7.6); this yields (5.1). This result is in agreement with the non-magnetic version of the velocity obtained by Moffatt & Loper (1994); see (2.8). The pressure is zero at the parcel centre by symmetry.

7.1. *Gravity and rotation antiparallel*

If gravity and rotation are antiparallel, (7.6) and (7.7) simplify to

$$\boldsymbol{u}(\boldsymbol{x}) = \tfrac{1}{2}\pi[(1-x_\perp^2)f_0(x_\perp) + x_\perp^2 f_1(x_\perp)]\hat{\boldsymbol{\Omega}} - \sqrt{\pi}\,\mathrm{erf}\,(x_\Omega)\exp(-x_\perp^2)\hat{\boldsymbol{\Omega}}\times\boldsymbol{x}_\perp \tag{7.8}$$

and

$$p(\boldsymbol{x}) = \tfrac{1}{2}\sqrt{\pi}\,\mathrm{erf}\,(x_\Omega)\exp(-x_\perp^2). \tag{7.9}$$

This flow consists of motion in the axial direction which extends beyond the lateral confines of the parcel plus a swirl within the lateral confines of the parcel. Outside the parcel, the Coriolis force of the swirl is balanced by the pressure gradient. Within the parcel, the Coriolis, pressure and buoyancy forces are in balance.

The structure of the axial flow as a function of radius, $x_\perp$, in the antiparallel case is given in figure 7. Also plotted for comparison is the exponential function $\exp(-x_\perp^2)$. The axial flow has the property that its area average is zero. This property necessarily requires a region of counter (downward) flow outside the primary Taylor column; this region occurs for $x_\perp > 1.257$ as seen in figure 7. This axial counter flow decays algebraically with radial distance from the parcel: $\boldsymbol{u}\cdot\hat{\boldsymbol{\Omega}} \sim -\sqrt{\pi}/4x_\perp^3$. This behaviour is in agreement with that deduced by Stewartson (1953; see his equation 5.10), although the numerical factors differ. Return flow in a broad region around the body has not been found in previous studies of Taylor columns, with the exception

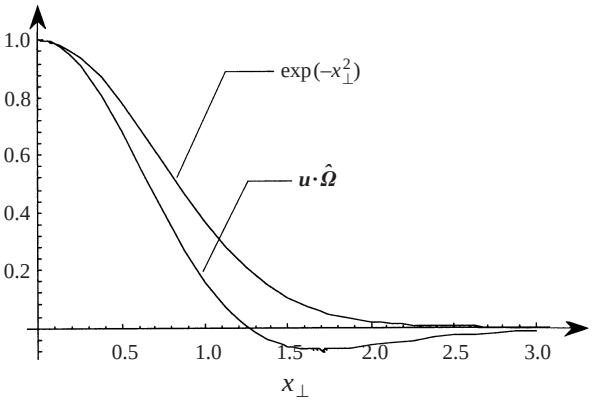

FIGURE 7. A graph of the axial velocity component in the vicinity of the parcel in the antiparallel case, together with the buoyancy function.

of the pioneering work of Stewartson (1952, 1953) and the study of Tanzosh & Stone (1994). In more recent studies, the return flow has been assumed to occur within thin Stewartson layers on the tangent cylinder; e.g. see Bush *et al.* (1995, figure 1). These layers do not arise in the case of flow driven by a buoyant parcel. In fact, the tangent cylinder cannot be defined for a parcel having a smooth distribution of buoyancy.

Outside the parcel, the pressure distribution given by (7.9) integrates to give a force

$$F_p = \operatorname{sgn}(x_\Omega)\pi^{3/2}/2, \tag{7.10}$$

which exactly balances the buoyancy force of the parcel.

7.2. *Comments on the structure and validity of the near-parcel solution*

The question naturally arises regarding the origin of the broad region of return flow in the vicinity of the parcel. It has been shown in § 6 that the fluid flow far from the parcel broadens with increasing distance, as dictated by the form of the similarity variable, ξ, defined by (6.1). It has also been shown that the axial velocity far from the parcel has a return flow; see figures 2 and 6(*a*). It is apparent from figure 2 that the broad return flow near the parcel is simply an axial continuation of the return flow far ahead of and far behind the parcel.

The flow and pressure near the buoyant parcel are independent of the Ekman number. As noted in § 2.2, this implies that these near-parcel solutions will remain valid if forces other than viscous balance the Coriolis force and that the solution presented in this section may have a larger range of validity than implied by constraint (1.3). This conjecture is beyond the scope of the present paper, and will be investigated subsequently.

Recall that the solutions presented § 6 are independent of the form of the buoyant parcel, and sensitive only to the total buoyancy. It is very plausible to surmise that those far-field solutions are valid for flow driven by a rigid body of identical buoyancy. In that case, it seems likely that the return flow in the vicinity of a rigid parcel will be broad, rather than concentrated in narrow Stewartson layers. This behaviour is in general agreement with Stewarston's (1952, 1953) analyses. The validity of this line of reasoning may be tested by solving equation (48) of Vedensky & Ungarish (1994) for the stream function in the equatorial plane outside the disk (i.e. for $z = 0$ and $r > 1$) in the limit $\mathscr{T} \gg 1$. This is not a trivial exercise.

8. Rise velocity

With the velocity in the vicinity of the parcel known explicitly it is straightforward, in principle, to calculate the rise velocity of the parcel. However, this exercise is complicated by the fact that there is more than one definition for this quantity. In a similar study, Moffatt & Loper (1994) chose to define the rise velocity as the velocity at the centre of the parcel. In what follows the rise velocity is defined as the average of the velocity, weighted by the buoyancy distribution:

$$\boldsymbol{U}_p = \frac{\int \Psi(\boldsymbol{x})\boldsymbol{u}(\boldsymbol{x})\,\mathrm{d}^3\boldsymbol{x}}{\int \Psi(\boldsymbol{x})\,\mathrm{d}^3\boldsymbol{x}}. \tag{8.1}$$

This definition is motivated by the realization that the flow is driven by the release of gravitational potential energy, $\mathscr{E}$, and that this may be expressed alternatively as a point-wise integral or as a macroscopic dot product of the buoyancy force and the rise velocity:

$$\mathscr{E} = \boldsymbol{F}\cdot\boldsymbol{U}_p = \left[\int \Psi(\boldsymbol{x})\hat{\boldsymbol{g}}\,\mathrm{d}^3\boldsymbol{x}\right]\cdot\boldsymbol{U}_p = \int \Psi(\boldsymbol{x})\boldsymbol{u}(\boldsymbol{x})\cdot\hat{\boldsymbol{g}}\,\mathrm{d}^3\boldsymbol{x}. \tag{8.2}$$

The velocity defined by (8.1) is easily evaluated; substituting (7.6) and (3.12) and integrating, gives

$$\boldsymbol{U}_p = -\frac{\sqrt{2}\pi}{16}[\hat{\boldsymbol{g}} + (\hat{\boldsymbol{\Omega}}\cdot\hat{\boldsymbol{g}})\hat{\boldsymbol{\Omega}}] + \frac{1}{2\sqrt{2}}\hat{\boldsymbol{\Omega}}\times\hat{\boldsymbol{g}}. \tag{8.3}$$

This velocity is in the same direction as that at the centre of the parcel (compare (8.3) with (5.1)), but is smaller by a factor $2\sqrt{2}$. The velocity consists of a motion in the meridional plane, represented by the first term on the right-hand side, plus an azimuthal motion, represented by the second term. The predicted trajectory in Earth's core lies on a parabola of revolution, as deduced by Moffatt & Loper (1994), based on the velocity at the parcel centre.

The out-of-plane motion in (8.3) is normal to the gravitational vector and so does not contribute to the rate of rise: the rise speed is given by the dot product of (8.3) with the unit gravity vector:

$$U = \tfrac{1}{16}\sqrt{2}\pi\sqrt{1 + 3(\hat{\boldsymbol{\Omega}}\cdot\hat{\boldsymbol{g}})^2}. \tag{8.4}$$

The rise speed is a maximum when $\boldsymbol{\Omega}$ and $\boldsymbol{g}$ are parallel or antiparallel; in this case,

$$U = \tfrac{1}{8}\sqrt{2}\pi \approx 0.5554. \tag{8.5}$$

8.1. *Comparison with the motion of rigid bodies*

It is instructive to compare and contrast the different velocity–drag formulas for flow driven by rigid bodies and fluid parcels. In rigid-body flow, a velocity is prescribed and the drag is calculated, while in parcel flow the force is prescribed and the velocity is calculated. In this subsection, the force–velocity relation for a rigid body will be inverted and compared with the velocity–force relation for a fluid parcel.

Introducing a Cartesian coordinate system with the z-axis parallel to the rotation axis, formulas (2.3), (2.5) and (2.6), quantifying the drag on a rigid body, may be

combined into a single matrix formula:

$$\begin{bmatrix} D_x \\ D_y \\ D_z \end{bmatrix} = -\frac{16}{3}\rho\Omega a^3 \begin{bmatrix} \dfrac{2\pi^2}{16+\pi^2} & \dfrac{\pi^3}{2(16+\pi^2)} & 0 \\ -\dfrac{\pi^3}{2(16+\pi^2)} & \dfrac{2\pi^2}{16+\pi^2} & 0 \\ 0 & 0 & 1 \end{bmatrix} \begin{bmatrix} U_x \\ U_y \\ U_z \end{bmatrix}; \tag{8.6}$$

see also formula (3.8) of Tanzosh & Stone (1995). Note that D and U are dimensional. The drag is equal and opposite to the buoyancy force on a freely moving sphere:

$$\boldsymbol{D}_s = \tfrac{4}{3}\pi(\Delta\rho)_s a_s^3 \boldsymbol{g}, \tag{8.7}$$

where $(\Delta\rho)_s$ is the (uniform) density deficit of the sphere and a_s is its radius. If the total force on the sphere is the same as the buoyancy force on the parcel, then $4(\Delta\rho)_s a_s^3 = 3\pi(\Delta\rho)a^3$.

The inverse of (8.6) and (8.7) may be combined into a force–velocity relation for a rigid body:

$$\begin{bmatrix} U_x \\ U_y \\ U_z \end{bmatrix} = -\frac{\pi}{4\Omega}\left(\frac{(\Delta\rho)_s}{\rho}\right) \begin{bmatrix} 8/\pi^2 & -2/\pi & 0 \\ 2/\pi & 8/\pi^2 & 0 \\ 0 & 0 & 1 \end{bmatrix} \begin{bmatrix} g_x \\ g_y \\ g_z \end{bmatrix}. \tag{8.8}$$

The corresponding dimensional matrix form of (8.3), quantifying the force–velocity relation for a fluid parcel, is

$$\begin{bmatrix} U_x \\ U_y \\ U_z \end{bmatrix} = -\frac{\sqrt{2}\pi}{16\Omega}\left(\frac{\Delta\rho}{\rho}\right) \begin{bmatrix} 1/2 & -2/\pi & 0 \\ 2/\pi & 1/2 & 0 \\ 0 & 0 & 1 \end{bmatrix} \begin{bmatrix} g_x \\ g_y \\ g_z \end{bmatrix}, \tag{8.9}$$

where $\Delta\rho$ is the maximum density deficit at the centre of the Gaussian parcel.

The rise speed is independent of the size of the body, but is sensitive to the magnitude of the density deficit. The axial speeds of the fluid and rigid bodies become identical if $\Delta\rho = 2\sqrt{2}(\Delta\rho)_s$. Alternatively if $\Delta\rho = (\Delta\rho)_s$, the axial speed of the fluid parcel is $\sqrt{2}/4$ times that of the sphere; it is more difficult for the fluid parcel to move axially. While the centre of the fluid parcel moves as fast as a rigid body having an identical density deficit, the remaining portions move more slowly for two reasons. First, they have a smaller density deficit. Second, the requirement of no net axial flow results in a negative axial speed at distances greater than 1.257; see figure 7. This sweeps the fringes of the buoyant parcel backward causing the net axial speed to be reduced.

The transverse speed of the fluid parcel is 50% of the axial speed, while the transverse speed of the sphere is 81% of the axial speed; the fluid parcel has an even more difficult time moving transversely. The lift force, as a fraction of the transverse drag is greater than unity ($4/\pi$) for the fluid parcel, but less than unity ($\pi/4$) for the rigid sphere; the fluid parcel veers off line more than the rigid sphere does during transverse motion.

The difference in velocities quantified by (5.1) and (8.3) is an indication that the parcel is deformed by the flow. The nature of that deformation is investigated in the following section.

9. Parcel deformation

It has been assumed that the parcel has a known and simple buoyancy distribution at a given instant of time. The flow generated by this buoyancy, given by (7.1) or equivalently (7.6), will deform the distribution. The purpose of this section is to quantify this deformation and motivate the choice of a new, more general and robust buoyancy distribution.

Ignoring molecular diffusion of buoyancy, the equation of conservation of buoyant constituent may be expressed as

$$\frac{\partial \Psi}{\partial t} = -\boldsymbol{u}_r \cdot \nabla \Psi, \tag{9.1}$$

where the relative velocity $\boldsymbol{u}_r$ is defined by (3.1) and $\boldsymbol{u}_l$ has been expressed as $\boldsymbol{u}$ in §§ 3–7. The time rate of change is measured by an observer moving with the centre of the parcel. The neglect of diffusion is justified provided $Ua \gg D$, where D is the coefficient of molecular diffusion. For many liquid systems $D \approx 10^{-9}\,\mathrm{m^2\,s^{-1}}$; this small value ensures that advection dominates diffusion in virtually all applications.

Combining (3.1), (7.6) and (8.3), yields

$$\begin{aligned}\boldsymbol{u}_r = &\left[\exp(-x^2) - \frac{1}{2\sqrt{2}}\right] \hat{\boldsymbol{\Omega}} \times \hat{\boldsymbol{g}} - \sqrt{\pi}\,\mathrm{erf}\,(x_\Omega)\exp(-x_\perp^2)\boldsymbol{x}_\perp \times \hat{\boldsymbol{g}} \\ &-\frac{\pi}{4}\left(f_0 - f_1 - \frac{\sqrt{2}}{4}\right)[\hat{\boldsymbol{g}} + (\hat{\boldsymbol{\Omega}} \cdot \hat{\boldsymbol{g}})\hat{\boldsymbol{\Omega}}] - \frac{\pi}{2}\left[f_0 - \left(1 + \frac{1}{x_\perp^2}\right) f_1\right] \boldsymbol{x}_\perp \times (\boldsymbol{x}_\perp \times \hat{\boldsymbol{g}}).\end{aligned} \tag{9.2}$$

Advection of buoyancy takes differing forms depending on whether gravity and rotation are aligned or not. These two cases are considered in turn in the following two subsections.

9.1. *Gravity and rotation antiparallel*

In this case, (9.2) simplifies to

$$\boldsymbol{u}_r = u(x_\perp)\hat{\boldsymbol{\Omega}} - \sqrt{\pi}\,\mathrm{erf}\,(x_\Omega)\exp(-x_\perp^2)\hat{\boldsymbol{\Omega}} \times \boldsymbol{x}_\perp, \tag{9.3}$$

where

$$u(x_\perp) = \tfrac{1}{2}\pi[(1 - x_\perp^2)f_0(x_\perp) + x_\perp^2 f_1(x_\perp) - \tfrac{1}{4}\sqrt{2}]. \tag{9.4}$$

The second factor on the right-hand side of (9.3) has no effect on an axisymmetric density distribution, while the first translates it in the axial direction. The resulting density distribution is

$$\Psi(\boldsymbol{x}, t) = \exp(-x_\perp^2 - [x_\Omega - u(x_\perp)t]^2). \tag{9.5}$$

The flow solution presented in § 7 is insensitive to the axial position of the buoyancy, provided that its axial scale is less than that of the Taylor column. In this case the momentum and material-advection equations are decoupled; a buoyant parcel of the form (9.5) will produce a velocity field identical to that presented in § 7, provided $|t| < O(1/E)$. That is, that the flow solution presented in this paper will remain valid in the antiparallel case as long as the parcel is not elongated as much as the Taylor column.

The horizontally averaged buoyancy, Ψ_h, quantified by

$$\Psi_h(x_\Omega, t) = \int_0^\infty \Psi(\boldsymbol{x}, t) 2x_\perp \mathrm{d}x_\perp, \tag{9.6}$$

is plotted as a function of vertical position in figure 8 for several values of time. The effect of fluid motion is to smear the buoyancy in the vertical direction.

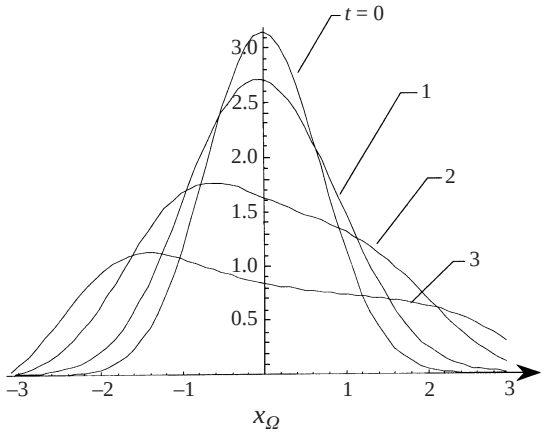

FIGURE 8. Profiles of Ψ_h versus x_Ω for several values of time.

9.2. *Gravity and rotation not aligned*

If rotation and gravity are not aligned, the situation is more complicated. Analysis of the flow is facilitated by the introduction of a Cartesian coordinate system aligned with rotation and gravity; let

$$\hat{\boldsymbol{g}} = -\cos(\theta)\hat{\boldsymbol{\Omega}} + \sin(\theta)\hat{\boldsymbol{g}}_\perp, \tag{9.7}$$

$$\hat{\boldsymbol{x}}_\perp = \cos(\phi)\hat{\boldsymbol{g}}_\perp + \sin(\phi)\hat{\boldsymbol{n}}, \tag{9.8}$$

where

$$\hat{\boldsymbol{n}} = \hat{\boldsymbol{\Omega}} \times \hat{\boldsymbol{g}}_\perp. \tag{9.9}$$

Now (9.2) may be written as

$$\boldsymbol{u}_r = u_\Omega \hat{\boldsymbol{\Omega}} + u_g \hat{\boldsymbol{g}}_\perp + u_n \hat{\boldsymbol{n}} \tag{9.10}$$

where

$$u_\Omega = \tfrac{1}{2}\pi[(1 - x_\perp^2)f_0 + x_\perp^2 f_1 - \tfrac{1}{4}\sqrt{2}]\cos(\theta) + \sqrt{\pi}\,\mathrm{erf}(x_\Omega)\exp(-x_\perp^2)\sin(\theta)\sin(\phi), \tag{9.11}$$

$$u_g = -\tfrac{1}{4}\pi\left[(2 - 2x_\perp^2)f_0 + \left(-\frac{1}{x_\perp^2} + 2x_\perp^2\right)f_1 - \tfrac{1}{4}\sqrt{2}\right]\sin(\theta)$$
$$+\sqrt{\pi}\,\mathrm{erf}(x_\Omega)\exp(-x_\perp^2)\cos(\theta)\sin(\phi) - \tfrac{1}{4}\pi\left[f_0 - \left(1 + \frac{1}{x_\perp^2}\right)f_1\right]\sin(\theta)\cos(2\phi) \tag{9.12}$$

and

$$u_n = \left[\exp(-x^2) - \frac{1}{2\sqrt{2}}\right]\sin(\theta) - \sqrt{\pi}\,\mathrm{erf}(x_\Omega)\exp(-x_\perp^2)\cos(\theta)\cos(\phi)$$
$$-\tfrac{1}{4}\pi\left[f_0 - \left(1 + \frac{1}{x_\perp^2}\right)f_1\right]\sin(\theta)\sin(2\phi). \tag{9.13}$$

The portions of the flow field involving sines or cosines of ϕ have no net effect on the buoyancy distribution; these will be ignored. The remaining flow consists of three

parts, quantified by the first terms on the right-hand sides of (9.11)–(9.13). The first two act to spread the parcel in the $(\hat{\boldsymbol{g}}, \hat{\boldsymbol{\Omega}})$-plane, much as the axial velocity component did in the case presented in § 9.1. The third is a motion out of the $(\hat{\boldsymbol{g}}, \hat{\boldsymbol{\Omega}})$-plane that is limited to the confines of the buoyancy distribution. This will result in a shift in the distribution, making it 'lopsided' but will not result in an overall change in the size of the parcel in that direction. These deformations may be approximately modelled with a buoyancy distribution of the form

$$\Psi(\boldsymbol{x}, t) = [1 + q(x_\perp, t)x_n] \exp(-x_n^2 - [x_\Omega - \xi_\Omega(x_\perp, t)]^2 - [x_g - \xi_g(x_\perp, t)]^2) \tag{9.14}$$

where $x_g = \boldsymbol{x} \cdot \hat{\boldsymbol{g}}_\perp, x_n = \boldsymbol{x} \cdot \hat{\boldsymbol{n}}$,

$$\xi_\Omega(x_\perp, 0) = \tfrac{1}{2}\pi[(1 - x_\perp^2)f_0 + x_\perp^2 f_1 - \tfrac{1}{4}\sqrt{2}] \cos(\theta) \tag{9.15}$$

and

$$\xi_g(x_\perp, 0) = \tfrac{1}{4}\pi \left[(2 - 2x_\perp^2)f_0 + \left(-\frac{1}{x_\perp^2} + 2x_\perp^2\right) f_1 - \frac{\sqrt{2}}{4}\right] \sin(\theta). \tag{9.16}$$

This deformation will be investigated in a subsequent study.

10. Summary and discussion

10.1. *Summary*

The quasi-steady velocity and pressure fields induced by a buoyant parcel of Gaussian shape rising in a rapidly rotating fluid of infinite extent have been investigated in the limit that the Ekman number is much smaller than unity and Rossby number is sufficiently small that the inertia terms may be neglected. The Ekman number is a small parameter which is used to advantage in obtaining an analytic solution.

The linear problem is simple to solve in Fourier transform space; the challenge is to invert the solution. An important contribution of this paper is to identify a procedure for inverting this solution. The essence of the procedure is to express the wavenumber vector in cylindrical coordinates, with the axial coordinate being parallel to the rotation vector. With this decomposition, angular inversion integrals can be performed exactly and axial inversion integrals can be carried out to any accuracy desired. The velocity and pressure are found to dominant, i.e. unit, order. In addition one term of order E, quantifying the small radial flow, is retained in the expression for the velocity. The most general and useful expressions for velocity and pressure are given by (4.20) and (4.21), which involve radial inversion integrals in $\boldsymbol{k}$-space.

The radial inversion integrals contain the radial and axial coordinates (in physical space) as parameters. These integrals have been represented graphically (involving a single physical spatial variable) along the modal axis (in § 5) and in the far Taylor column (in § 6). Moreover, these integrals can be evaluated analytically near the parcel; the velocity and pressure in the vicinity of the parcel are found *entirely in closed form* (in § 7).

The velocity along the modal axis consists of a motion out of the $(\hat{\boldsymbol{g}}, \hat{\boldsymbol{\Omega}})$-plane which is confined to the axial extent of the parcel and a motion in that plane which varies on the scale of the Taylor column. Both these motions are even functions of the axial coordinate. The pressure on the modal axis consists of a single term which varies on both the scale of the parcel and the scale to the Taylor column. This pressure is an odd function of the axial coordinate. Outside the parcel, the magnitudes of the velocity and pressure decrease rapidly in magnitude relatively close to the parcel,

reaching half their maximum values at $E|x_\Omega| \approx 0.055$ and 0.094, respectively; see figure 5. The velocity on the modal axis has no recirculating 'Taylor slug' such as occurs in the case of forcing by a rigid body (Maxworthy 1970; Vedensky & Ungarish 1994). In spite of the rapid initial decrease in magnitude, the velocity and pressure on the modal axis decay algebraically at large axial distance, varying as $1/E|x_\Omega|$ and $1/(E|x_\Omega|)^{2/3}$, respectively; see (5.12) and (5.13).

The velocity and pressure off the modal axis and far from the parcel are functions of the similarity variable, $\xi = x_\perp/(E|x_\Omega|)^{1/3}$, divided by $1/E|x_\Omega|$ and $1/(E|x_\Omega|)^{2/3}$, respectively. The velocity and pressure fields decay algebraically with increasing distance from the parcel, as quantified by either variable. The integral of the pressure over an area normal to the rotation axis is independent of axial distance and the resulting pressure force balances the buoyancy of the parcel.

The analytic solutions for velocity and pressure in the vicinity of the parcel that are presented in § 7 quantify a baroclinic balance within the parcel and a geostrophic balance outside. The geostrophic balance satisfies the Taylor–Proudman theorem at dominant order in powers of E. It is readily seen from (7.1) and (7.2) that there are two distinct geostrophic balances, involving both velocity and pressure, which are characterized by the radial extent of the associated variables and which depend on the relative orientation of rotation and gravity. One balance occurs on the axial extension of the parcel, and is associated with the swirl quantified by the first term on the right-hand side of (7.1) (or the second of (7.6)). The other balance has a much larger radial extent and involves the modulated radial motion, quantified by the second term on the right-hand side of (7.1) (or the fourth of (7.6)). The remaining geostrophic portion of the velocity, i.e. the last term of (7.1), represents rectilinear return flow, necessary to satisfy conservation of mass, and being rectilinear does not require a balancing pressure field. In the case that rotation and gravity are aligned, the azimuthal modulation is absent.

The rise velocity of the parcel, quantified in § 8, is found to be significantly smaller than the velocity of the parcel centre, albeit in the same direction. The fluid parcel moves significantly more slowly than a rigid body having a density contrast equal to the maximum of the parcel, but experiences a larger relative lift force than does a rigid body.

The parcel is strongly deformed by the flow, but this deformation has little effect when gravity and rotation are aligned. This deformation is quantified in § 9.1. In the general case the solution presented in this paper is strictly valid only for times short compared with the advection time due to deformation. However, the solution far from the parcel is insensitive to the precise form of the parcel, and depends predominantly on the total buoyancy.

10.2. *Discussion*

The solution procedure presented in this paper is a significant step toward realistic quantification of the flow and pressure associated with small-scale buoyant structures in large fluid bodies, such as the Earth's outer core or fluid portions of other heavenly bodies, as well as in rapidly rotating systems such as centrifuges. However, the present solution has many limitations.

One serious limitation on the solution is inequality (1.3). The present procedure can be generalized to include a linearized (Oseen-like) version of the inertia terms, significantly increasing the range of validity of the solution. This step should be relatively straightforward and is being undertaken at present.

Another limitation on the present solution is that it is kinematic, with the structure

of the buoyant parcel fixed and prescribed. The flow field in the vicinity of the parcel is complex, so a complete quantification of its effects would be quite difficult. However, the gross effects of parcel deformation appear to be quantifiable.

A third limitation on the present solution is the assumption of steady flow. This is reasonable for laboratory experiments having rapid rotation; however, it is a strong limitation on natural geophysical flows. Unsteady effects need to be incorporated. The initial-value problem might be tackled following the leads of Smith (1983) and Price & Tan (1992).

The procedure described in this paper was initially discovered in the attempt to solve the corresponding hydromagnetic problem, with application to the form of small-scale flows in the outer core of the Earth. Hydromagnetic effects can be easily added to the present formulation.

This work was supported in part by the National Science Foundation under grant # EAR-9417481 and is contribution #417 of the Geophysical Fluid Dynamics Institute.

Appendix A. Limits of validity of the linearized solution

The purpose of this appendix is to quantify the limits of the linearized analysis of the main text. The full, nonlinear momentum equation may be expressed in dimensionless form as

$$\hat{\boldsymbol{\Omega}} \times \boldsymbol{u} + \nabla p = -\Psi \hat{\boldsymbol{g}} + E\nabla^2 \boldsymbol{u} + R_o[\boldsymbol{U}_p - \boldsymbol{u}] \cdot \left[\hat{\boldsymbol{\Omega}} \frac{\partial \boldsymbol{u}}{\partial x_\Omega} + \nabla_\perp \boldsymbol{u}\right]. \tag{A 1}$$

The terms on the left-hand side, representing the geostropic forces, are balanced by those on the right-hand side, representing buoyancy, viscous and inertial forces, respectively. The conditions under which the inertial force is negligibly small compared with either the buoyancy or viscous force are to be determined.

Within the parcel, where the buoyancy force is of unit order, it is sufficient that R_o be small compared with unity. The more stringent condition is that which involves the structure of the Taylor column, outside the parcel, i.e. where $\Psi \approx 0$. This structure is determined by small but cumulative departures from the geostrophic balance due to the action of the viscous force, which is of order E. Within the Taylor column axial derivatives are of order E while velocities are of unit order. It follows that the condition $R_o \ll 1$ is sufficient to ensure that the axial inertial term, $R_o[\boldsymbol{U}_p - \boldsymbol{u}] \cdot \hat{\boldsymbol{\Omega}} \partial \boldsymbol{u}/\partial \boldsymbol{x}_\Omega$, is negligibly small. It remains to quantify the transverse inertial term, $R_o[\boldsymbol{U}_p - \boldsymbol{u}] \cdot \nabla_\perp \boldsymbol{u}$. Although the fluid velocity in the Taylor column is nominally of unit order for a distance of order $1/E$ from the parcel, it is seen in § 5 (see figure 5) that the velocity in fact decays rapidly, leaving the dominant portion of the transverse inertial term, $R_o[\boldsymbol{U}_p \cdot \nabla_\perp]\boldsymbol{u}$, to be quantified. Using (8.3),

$$\boldsymbol{U}_p \cdot \nabla_\perp = -\frac{\sqrt{2}\pi}{16} \hat{\boldsymbol{g}} \cdot \nabla_\perp. \tag{A 2}$$

This expression is of order $\sin\theta$ where θ is the colatitude. The transverse inertial term is of order $R_o \sin\theta$ and is smaller than the viscous term provided $R_o \sin\theta \ll E$. Since both terms being compared (i.e. $R_o[\boldsymbol{U}_p \cdot \nabla_\perp]\boldsymbol{u}$ and $E\nabla_\perp^2 \boldsymbol{u}$) are linear in the velocity vector, $\boldsymbol{u}$, this condition on Rossby number is uniformly valid.

Appendix B. Evaluation of Fourier integrals

The purpose of this appendix is to evaluate the Fourier inversion integrals in the angular and axial directions. The integrals to be evaluated may be obtained by substituting (3.13) and (4.1) into (3.11) and thence into (3.10). The result may be expressed as

$$\boldsymbol{u}(\boldsymbol{x}) = \frac{1}{8\pi^{3/2}} \int_0^\infty \boldsymbol{v}(k_\perp; x_\Omega, \boldsymbol{x}_\perp) \exp\left(-\frac{k_\perp^2}{4}\right) k_\perp \mathrm{d}k_\perp, \tag{B 1}$$

with

$$\boldsymbol{v}(k_\perp; x_\Omega, \boldsymbol{x}_\perp) = \int_{-\infty}^\infty \frac{\boldsymbol{w}(k_\perp, k_\Omega; \boldsymbol{x}_\perp)}{k_\Omega^2 + E^2 k_\perp^6} \exp\left(-\mathrm{i} x_\Omega k_\Omega - \frac{k_\Omega^2}{4}\right) \mathrm{d}k_\Omega, \tag{B 2}$$

and

$$\boldsymbol{w}(k_\perp, k_\Omega; \boldsymbol{x}_\perp) = Ek_\perp^2 [k_\Omega k_\perp \hat{\boldsymbol{\Omega}} \times (\boldsymbol{y}_2 \times \hat{\boldsymbol{g}}) + k_\perp^2 \boldsymbol{y}_3] + [k_\Omega^2 y_1 \hat{\boldsymbol{\Omega}} + k_\Omega k_\perp \boldsymbol{y}_2] \times [\hat{\boldsymbol{g}} + Ek_\perp^2 (\hat{\boldsymbol{\Omega}} \times \hat{\boldsymbol{g}})] \tag{B 3}$$

where

$$y_1(k_\perp; \boldsymbol{x}_\perp) = \int_{-\pi}^{\pi} \exp(-\mathrm{i} k_\perp x_\perp \hat{\boldsymbol{k}}_\perp \cdot \hat{\boldsymbol{x}}_\perp) \, \mathrm{d}\phi, \tag{B 4}$$

$$\boldsymbol{y}_2(k_\perp; \boldsymbol{x}_\perp) = \int_{-\pi}^{\pi} \hat{\boldsymbol{k}}_\perp \exp(-\mathrm{i} k_\perp x_\perp \hat{\boldsymbol{k}}_\perp \cdot \hat{\boldsymbol{x}}_\perp) \, \mathrm{d}\phi, \tag{B 5}$$

and

$$y_3(k_\perp; \boldsymbol{x}_\perp) = \int_{-\pi}^{\pi} \hat{\boldsymbol{k}}_\perp \times (\hat{\boldsymbol{k}}_\perp \times \hat{\boldsymbol{g}}) \exp(-\mathrm{i} k_\perp x_\perp \hat{\boldsymbol{k}}_\perp \cdot \hat{\boldsymbol{x}}_\perp) \, \mathrm{d}\phi. \tag{B 6}$$

The integration in the angular direction is performed exactly in § B.1. The axial integration may be performed to any order, in integer powers of E, desired. The axial integrals to dominant order plus the radial velocity component (at order E) are evaluated in § B.2. One of the resulting five radial integrals may be evaluated exactly; see § B.3.

B.1. *Evaluation of the angular Fourier integral*

Define ϕ as the angle from the projection of $\boldsymbol{x}$ onto the $\boldsymbol{k}_\perp$-plane, so that

$$\hat{\boldsymbol{k}}_\perp = \cos(\phi) \hat{\boldsymbol{x}}_\perp + \sin(\phi) \hat{\boldsymbol{\Omega}} \times \hat{\boldsymbol{x}}_\perp. \tag{B 7}$$

Making use of symmetry and of Gradshteyn & Rhyzik (1980, formulas 3.715.13 and 3.715.18, p. 402 plus their derivatives), the angular integrals may be expressed as

$$y_1 = 2\pi J_0(x_\perp k_\perp), \tag{B 8}$$

$$\boldsymbol{y}_2 = -2\pi \mathrm{i} J_1(x_\perp k_\perp) \hat{\boldsymbol{x}}_\perp \tag{B 9}$$

and

$$\boldsymbol{y}_3 = -\frac{2\pi}{x_\perp k_\perp} J_1(x_\perp k_\perp) [\hat{\boldsymbol{g}} + (\hat{\boldsymbol{g}} \cdot \hat{\boldsymbol{\Omega}}) \hat{\boldsymbol{\Omega}}] - 2\pi J_2(x_\perp k_\perp) \hat{\boldsymbol{x}}_\perp \times (\hat{\boldsymbol{x}}_\perp \times \hat{\boldsymbol{g}}), \tag{B 10}$$

where J_n is a Bessel function of order n. The first of the three inversions in $\boldsymbol{k}$-space is completed and the function $\boldsymbol{w}(k_\perp, k_\Omega; \boldsymbol{x}_\perp)$ has been determined without approximation.

B.2. *Evaluation of the axial Fourier integral*

To reduce the complexity of the mathematical expressions, in what follows those terms deriving from (B 3) which are of dominant (unit) order in powers of E and

those of order E which are involved in satisfaction of conservation of mass (i.e. the cylindrical radial velocity) will be retained. That is, (B 3) will be simplified to

$$\boldsymbol{w}(k_\perp, k_\Omega; \boldsymbol{x}_\perp) = Ek_\perp^3 k_\Omega \hat{\boldsymbol{\Omega}} \times (\boldsymbol{y}_2 \times \hat{\boldsymbol{g}}) + Ek_\perp^4 \boldsymbol{y}_3 + k_\Omega^2 y_1 \hat{\boldsymbol{\Omega}} \times \hat{\boldsymbol{g}} + k_\Omega k_\perp \boldsymbol{y}_2 \times \hat{\boldsymbol{g}}. \tag{B 11}$$

Higher-order accuracy in powers of E may be achieved at the cost of increased algebraic complexity. Since $y_1, \boldsymbol{y}_2$ and $\boldsymbol{y}_3$ are independent of x_Ω, the result of substituting (B 11) into (B 2) may be expressed as

$$\boldsymbol{v}(k_\perp; x_\Omega, \boldsymbol{x}_\perp) = Ek_\perp^3 \hat{\boldsymbol{\Omega}} \times (\boldsymbol{y}_2 \times \hat{\boldsymbol{g}}) V_1 + Ek_\perp^4 \boldsymbol{y}_3 V_0 + y_1 (\hat{\boldsymbol{\Omega}} \times \hat{\boldsymbol{g}}) V_2 + k_\perp (\boldsymbol{y}_2 \times \hat{\boldsymbol{g}}) V_1 \tag{B 12}$$

where

$$V_n(k_\perp; \boldsymbol{x}_\Omega) = \int_{-\infty}^{\infty} \frac{k_\Omega^n}{k_\Omega^2 + E^2 k_\perp^6} \exp\left(-\mathrm{i} x_\Omega k_\Omega - \frac{k_\Omega^2}{4}\right) \mathrm{d}k_\Omega. \tag{B 13}$$

Using Gradshteyn & Rhyzik (1980, formula 3.952.4, p. 495)

$$V_2 = 2\sqrt{\pi} \exp(-x_\Omega^2) - E^2 k_\perp^6 V_0. \tag{B 14}$$

Since $V_0 = O(1/E) \gg 1$ (see (B 21)), it is necessary to retain the last term in (B 14) to maintain accuracy at order E. Substituting (B 14) into (B 12) and discarding terms of order E^2, leads to

$$\boldsymbol{v}(k_\perp; x_\Omega, \boldsymbol{x}_\perp) = Ek_\perp^3 \hat{\boldsymbol{\Omega}} \times (\boldsymbol{y}_2 \times \hat{\boldsymbol{g}}) V_1 + Ek_\perp^4 \boldsymbol{y}_3 V_0 + y_1 (\hat{\boldsymbol{\Omega}} \times \hat{\boldsymbol{g}}) 2\sqrt{\pi} \exp(-x_\Omega^2)$$
$$- y_1 (\hat{\boldsymbol{\Omega}} \times \hat{\boldsymbol{g}}) E^2 k_\perp^6 V_0 + k_\perp (\boldsymbol{y}_2 \times \hat{\boldsymbol{g}}) V_1. \tag{B 15}$$

It remains to evaluate V_0 and V_1. Folding the integrals about $k_\Omega = 0$,

$$V_0 = 2 \int_0^{\infty} \frac{\cos(k_\Omega x_\Omega) \exp(-k_\Omega^2/4)}{k_\Omega^2 + E^2 k_\perp^6} \mathrm{d}k_\Omega \tag{B 16}$$

and

$$V_1 = -2\mathrm{i} \int_0^{\infty} \frac{\sin(k_\Omega x_\Omega) \exp(-k_\Omega^2/4)}{k_\Omega^2 + E^2 k_\perp^6} k_\Omega \mathrm{d}k_\Omega. \tag{B 17}$$

Note that V_0 is even and V_1 is odd in x_Ω. These integrals may be evaluated using Gradshteyn & Ryzhik (1980, formulas 3.954.1 and 3.954.2 on p. 497 with $\beta = 1/4$, $a = x_\Omega$ and $\gamma = Ek_\perp^3$). Without approximation, the results are

$$V_0 = \frac{\pi \exp(E^2 k_\perp^6/4)}{2Ek_\perp^3} \left[2\cosh(Ex_\Omega k_\perp^3) + \frac{\mathrm{erf}(x_\Omega - Ek_\perp^3/2)}{\exp(Ex_\Omega k_\perp^3)} - \frac{\mathrm{erf}(x_\Omega + Ek_\perp^3/2)}{\exp(-Ex_\Omega k_\perp^3)}\right] \tag{B 18}$$

and

$$V_1 = \frac{\mathrm{i}\pi \exp(E^2 k_\perp^6/4)}{2} \left[2\sinh(Ex_\Omega k_\perp^3) - \frac{\mathrm{erf}(x_\Omega - Ek_\perp^3/2)}{\exp(Ex_\Omega k_\perp^3)} - \frac{\mathrm{erf}(x_\Omega + Ek_\perp^3/2)}{\exp(-Ex_\Omega k_\perp^3)}\right]. \tag{B 19}$$

Note that $\exp(E^2 k_\perp^6/4) \approx 1 + O(E^2)$; also,

$$\mathrm{erf}(x_\Omega \pm Ek_\perp^3/2) \approx \mathrm{erf}(x_\Omega) \pm \frac{1}{\sqrt{\pi}} Ek_\perp^3 \exp(-x_\Omega^2) + O(E^2). \tag{B 20}$$

Now

$$V_0 \approx \frac{\pi}{Ek_\perp^3} H_c - \sqrt{\pi} \exp(-x_\Omega^2) + O(E) \tag{B 21}$$

and

$$V_1 = \mathrm{i}\pi H_s + O(E^2), \tag{B 22}$$

where (from (4.6) and (4.7))

$$H_c(k_\perp; x_\Omega) = \cosh(Ex_\Omega k_\perp^3) - \mathrm{erf}(x_\Omega)\sinh(Ex_\Omega k_\perp^3)$$

and

$$H_s(k_\perp; x_\Omega) = \sinh(Ex_\Omega k_\perp^3) - \mathrm{erf}(x_\Omega)\cosh(Ex_\Omega k_\perp^3).$$

Substitution of (B 21) and (B 22) into (B 15) yields

$$\begin{aligned}\boldsymbol{v}(k_\perp; x_\Omega, \boldsymbol{x}_\perp) = {} & \mathrm{i}\pi E k_\perp^3 H_s \hat{\boldsymbol{\Omega}} \times (\boldsymbol{y}_2 \times \hat{\boldsymbol{g}}) + [\pi k_\perp H_c - \sqrt{\pi} k_\perp^4 \exp(-x_\Omega^2)]\boldsymbol{y}_3 \\ & + [2\sqrt{\pi}\exp(-x_\Omega^2) - \pi E k_\perp^3 H_c] y_1 (\hat{\boldsymbol{\Omega}} \times \hat{\boldsymbol{g}}) + \mathrm{i}\pi k_\perp (\boldsymbol{y}_2 \times \hat{\boldsymbol{g}}) H_s. \end{aligned} \tag{B 23}$$

Again, to simplify the analysis, the terms within the square brackets of (B 23) which are of order E will be discarded. Using (B 8)–(B 10),

$$\begin{aligned}\boldsymbol{v}(k_\perp; x_\Omega, \boldsymbol{x}_\perp) = {} & 4\pi^{3/2}\exp(-x_\Omega^2) J_0(x_\perp k_\perp)(\hat{\boldsymbol{\Omega}} \times \hat{\boldsymbol{g}}) \\ & + 2\pi^2 E k_\perp^3 H_s J_1(x_\perp k_\perp)\hat{\boldsymbol{\Omega}} \times (\hat{\boldsymbol{x}}_\perp \times \hat{\boldsymbol{g}}) + 2\pi^2 k_\perp H_s J_1(x_\perp k_\perp)(\hat{\boldsymbol{x}}_\perp \times \hat{\boldsymbol{g}}) \\ & - \frac{2\pi^2}{x_\perp} H_c J_1(x_\perp k_\perp)[\hat{\boldsymbol{g}} + (\hat{\boldsymbol{g}} \cdot \hat{\boldsymbol{\Omega}})\hat{\boldsymbol{\Omega}}] - 2\pi^2 k_\perp H_c J_2(x_\perp k_\perp)\hat{\boldsymbol{x}}_\perp \times (\hat{\boldsymbol{x}}_\perp \times \hat{\boldsymbol{g}}). \end{aligned} \tag{B 24}$$

This completes the second of the three integrals in $\boldsymbol{k}$-space.

B.3. *Radial Fourier integrals*

Substitution of (B 24) into (B 1) yields five radial integrals. One of these is easily evaluated using Watson (1966, formula 13.3(4), p. 394 with $a = x_\perp$, $p^2 = 1/4$, and $\nu = 0$):

$$\int_0^\infty J_0(x_\perp k_\perp)\exp\left(-\frac{k_\perp^2}{4}\right) k_\perp \mathrm{d}k_\perp = 2\exp(-x_\perp^2). \tag{B 25}$$

Using this, (B 1) may be expressed as (4.3).

Appendix C. Integration of the pressure equation

The purpose of this appendix is to integrate (4.9) to obtain the pressure field. The first step in this process is to eliminate the terms involving the Laplacian. It is straightforward to verify that

$$\nabla_\perp^2 V_{s12} = \frac{8}{\sqrt{\pi}} x_\Omega x_\perp \exp(-x^2) + \frac{1}{x_\perp^2} V_{s12} - V_{s14} \tag{C 1}$$

and

$$\nabla_\perp^2 V_{c02} = -V_{c04}. \tag{C 2}$$

Also

$$\nabla_\perp^2 (\hat{\boldsymbol{g}} \times \hat{\boldsymbol{\Omega}} \cdot \hat{\boldsymbol{x}}_\perp) = -\frac{1}{x_\perp^2}(\hat{\boldsymbol{g}} \times \hat{\boldsymbol{\Omega}} \cdot \hat{\boldsymbol{x}}_\perp). \tag{C 3}$$

Using (C 1)–(C 3), (4.9) may be expressed as

$$\frac{\partial p}{\partial x_\Omega} = [E V_{c04} - \exp(-x^2)][\hat{\boldsymbol{g}} \cdot \hat{\boldsymbol{\Omega}}] + E\left[\frac{8}{\sqrt{\pi}} x_\Omega x_\perp \exp(-x^2) - V_{s14}\right][\hat{\boldsymbol{g}} \times \hat{\boldsymbol{\Omega}} \cdot \hat{\boldsymbol{x}}_\perp]. \tag{C 4}$$

The third term on the right-hand side of (C 4) contributes a small factor, of order E, to the pressure because it has a limited axial extent; this term will be ignored. However, the first and fourth terms contribute unit-order factors to the pressure because of their large axial extent.

The second step in integrating (4.9), now written as (C 4), is to express the integrals V_{cmn} and V_{smn} in terms of derivatives with respect to x_Ω. Combining derivatives of (4.6) and (4.7) plus (B 25), (4.4) and (4.5), yields

$$EV_{c04} = \frac{\partial V_{s01}}{\partial x_\Omega} + \exp(-x^2) \tag{C 5}$$

and

$$EV_{s14} = \frac{\partial V_{c11}}{\partial x_\Omega} + \frac{E}{2} x_\Omega \exp(-x_\Omega^2) \int_0^\infty J_1(x_\perp k_\perp) \exp\left(-\frac{k_\perp^2}{4}\right) k_\perp \mathrm{d}k_\perp. \tag{C 6}$$

The second term on the right-hand side of (C 6) makes a contribution of order E to the pressure; it may be neglected at dominant order. Equation (C 4) may now be rewritten using (C 5) and (C 6); at dominant order this is

$$\frac{\partial p}{\partial x_\Omega} = \frac{\partial}{\partial x_\Omega}(V_{s01}[\hat{\boldsymbol{g}} \cdot \hat{\boldsymbol{\Omega}}] - V_{c11}[\hat{\boldsymbol{g}} \times \hat{\boldsymbol{\Omega}} \cdot \hat{\boldsymbol{x}}_\perp]). \tag{C 7}$$

This equation is easily integrated and yields (4.10). Note that this solution satisfies the condition that $p \to 0$ as $x_\Omega \to \pm\infty$.

REFERENCES

Batchelor, G. K. 1967 *An Introduction to Fluid Dynamics*. Cambridge University Press.

Bush, J. W. M., Stone, H. A. & Bloxham, J. 1992 The motion of an inviscid drop in a bounded rotating fluid. *Phys. Fluids* A **4**, 1142–1147.

Bush, J. W. M., Stone, H. A. & Bloxham, J. 1995 Axial drop motion in rotating fluids. *J. Fluid Mech.* **282**, 247–278.

Childress, S. 1964 The slow motion of a sphere in a rotating, viscous fluid. *J. Fluid Mech.* **20**, 305–314.

Gradshteyn, I. S. & Ryzhik, I. M. 1980 *Table of Integrals, Series and Products*. Academic.

Greenspan, H. P. 1968 *The Theory of Rotating Fluids*. Cambridge University Press.

Herron, I. H., Davis, S. H. & Bretherton, F. P. 1975 On the sedimentation of a sphere in a centrifuge. *J. Fluid Mech.* **68**, 209–234.

Hide, R., Ibbetson, A. & Lighthill, M. J. 1968 On slow transverse flow past obstacles in a rapidly rotating fluid. *J. Fluid Mech.* **32**, 251–272.

Long, R. R. 1953 Steady motion around a symmetrical obstacle moving along the axis of a rotating liquid. *J. Met.* **10**, 197–202.

Maxworthy, T. 1970 The flow created by a sphere moving along the axis of a rotating, slightly viscous fluid. *J. Fluid Mech.* **40**, 453–479.

Moffatt, H. K. & Loper, D. E. 1994 The magnetostrophic rise of a buoyant parcel in the Earth's core. *Geophys. J. Intl* **117**, 394–402.

Moore, D. W. & Saffman, P. G. 1968 The rise of a body through a rotating fluid in a container of finite length. *J. Fluid Mech.* **31**, 635–642.

Moore, D. W. & Saffman, P. G. 1969 The structure of free vertical shear layers in a rotating fluid and the motion produced by a slowly rising body. *Phil. Trans. R. Soc. Lond.* A **264**, 597–634.

Price, W. G. & Tan, M.-Y. 1992 Fundamental viscous solutions or transient oseenlets associated with a body manoeuvering in a viscous fluid. *Proc. R. Soc. Lond.* A **438**, 447–466.

Pritchard, W. G. 1969 The motion generated by a body moving along the axis of a uniformly rotating fluid. *J. Fluid Mech.* **39**, 443–464.

Proudman, J. 1916 On the motions of solids in a liquid possessing vorticity. *Proc. R. Soc. Lond.* A **92**, 408–424.

Smith, S. H. 1983 On a point source in a rotating fluid. *J. Engng Maths* **17**, 257–262.

Stewartson, K. 1952 On the slow motion of a sphere along the axis of a rotating fluid. *Proc. Camb. Phil Soc*. **48**, 168–177.

Stewartson, K. 1953 On the slow motion of an ellipsoid in a rotating fluid. *Q. J. Mech. Appl. Maths* **6**, 141–162.

Stewartson, K. 1957 On almost rigid rotations. *J. Fluid Mech.* **3**, 17–26.

Tanzosh, J. P. & Stone, H. A. 1994 Motion of a rigid particle in a rotating viscous flow: an integral equation approach. *J. Fluid Mech.* **275**, 225–256.

Tanzosh, J. P. & Stone, H. A. 1995 Transverse motion of a disk through a rotating viscous fluid. *J. Fluid Mech.* **301**, 295–324.

Taylor, G. I. 1922 The motion of a sphere in a rotating liquid. *Proc. R. Soc. Lond*. A **102**, 180–189.

Taylor, G. I. 1923 Experiments on the motion of solid bodies in rotating fluids. *Proc. R. Soc. Lond*. A **104**, 213–219.

Tranter, C. J. 1966 *Integral Transforms in Mathematical Physics*. Methuen.

Ungarish, M. & Vedensky, D. 1995 The motion of a rising disk in a rotating axially bounded fluid for large Taylor number. *J. Fluid Mech.* **291**, 1–32.

Vedensky, D. & Ungarish, M. 1994 The motion generated by a slowly rising disk in an unbounded rotating fluid for arbitrary Taylor number. *J. Fluid Mech.* **262**, 1–26.

Watson, G. N. 1966 *A Treatise on the Theory of Bessel Functions*. Cambridge University Press.

Weisenborn, A. J. 1985 The drag on a sphere moving slowly in a rotating viscous fluid. *J. Fluid Mech.* **153**, 215–227.